



Research article

The active components of Erzhi wan and their anti-Alzheimer's disease mechanisms determined by an integrative approach of network pharmacology, bioinformatics, molecular docking, and molecular dynamics simulation

Meng Yu ^{a,1}, Zhongqi Shen ^{b,1}, Shaozhi Zhang ^a, Yang Zhang ^a, Hongwei Zhao ^{a,**}, Longfei Zhang ^{c,*}

^a Innovative Institute of Chinese Medicine and Pharmacy, Shandong University of Traditional Chinese Medicine, Jinan, Shandong, 250355, China

^b Institute of Chinese Medical Literature and Culture, Shandong University of Traditional Chinese Medicine, Jinan, Shandong, 250355, China

^c Experimental Center, Shandong University of Traditional Chinese Medicine, Jinan, Shandong, 250355, China

ARTICLE INFO

Keywords:

Erzhi wan
AD pathology
p53/PI3K/Akt signaling pathway
Oxidative stress
Network pharmacology
Computational biology

ABSTRACT

Erzhi Wan (EZW), a classic Traditional Chinese Medicine formula, has shown promise as a potential therapeutic option for Alzheimer's disease (AD), yet its mechanism remains elusive. Herein, we employed an integrative *in-silico* approach to investigate the active components and their mechanisms against AD. We screened four active components with blood-brain barrier permeabilities from TCMSP, along with 307 corresponding targets predicted by SwissTargetPrediction, PharmMapper, and TCMBank websites. Then, we retrieved 2260 AD-related targets from Genecards, OMIM, and NCBI databases. Furthermore, we constructed the protein-protein interaction (PPI) network of the intersected targets via the STRING database and performed the GO and KEGG enrichment analyses using the "clusterProfiler" R package. The results showed that the intersected targets were intimately related to the p53/PI3K/Akt signaling pathway, serotonergic synapse, and response to oxygen level. Subsequently, 25 core targets were found differentially expressed in brain regions by bioinformatics analyses of GEO datasets of clinical samples from the Alzdata database. The binding sites and stabilities between the active components and the core targets were investigated by the molecular docking approach using Autodock 4.2.6 software, followed by pocket detection and druggability assessment via the DoGSiteScorer server. The results showed that acacetin, β -sitosterol, and 3-O-acetyldammareneediol-II strongly interacted with the druggable pockets of AR, CASP8, POLB, and PREP. Eventually, the docking results were further cross-referenced with the literature research and validated by 100 ns of molecular dynamics simulations using GROMACS software. Binding free energies were calculated via MM/PBSA strategy combined with interaction entropy. The simulation results indicated stable bindings between four docking pairs including acacetin-AR, acacetin-CASP8, β -sitosterol-POLB, and 3-O-acetyldammareneediol-II-PREP. Overall, our study demonstrated a theoretical basis for how three active components of EZW confer efficacy against

* Corresponding author.

** Corresponding author.

E-mail addresses: 60011995@sducm.edu.cn (H. Zhao), longfei_zhang@sducm.edu.cn (L. Zhang).

¹ M. Yu and Z. Q. Shen contributed equally to this work.

AD. It provides a promising reference for subsequent research regarding drug discoveries and clinical applications.

1. Introduction

Alzheimer’s disease (AD), the leading cause of dementia in the elderly population, is an irreversible neurodegenerative brain

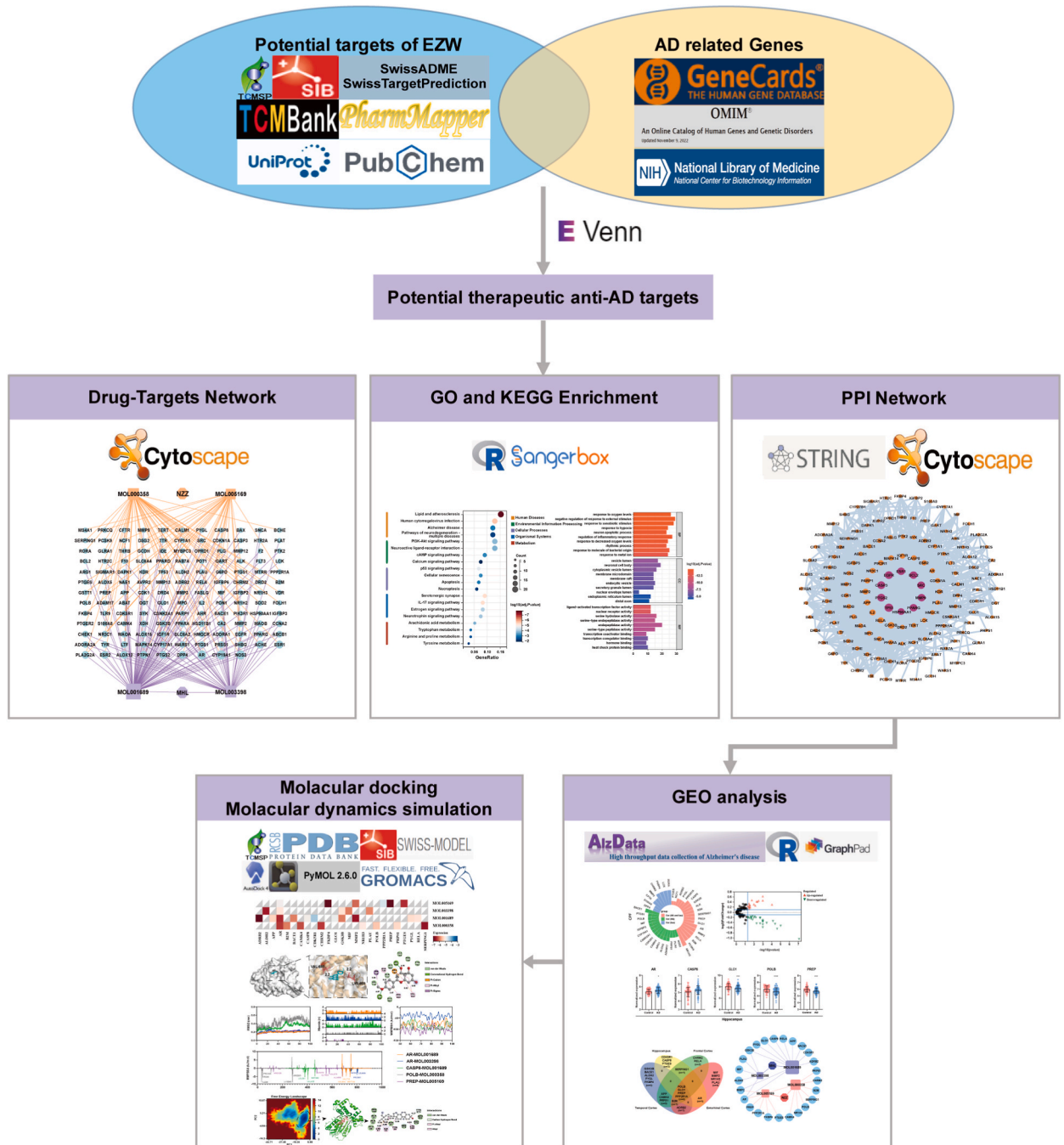


Fig. 1. The workflow of the integrated computational approach to study the mechanism of Erzhi Wan (EZW) against Alzheimer’s disease (AD). The workflow contains four sections including target screening from database retrieval, network construction and analysis, bioinformatics analysis upon Gene Expression Omnibus (GEO) datasets, and molecular docking and molecular dynamics simulation verifications.

disorder affecting more than 50 million people worldwide [1]. Individuals with the disease usually experience a relentless decline in memory and cognition to an extent that sufficiently interferes with daily life [2]. Despite its immense societal and economic impact, current Food and Drug Administration (FDA) approved medications can only alleviate symptoms rather than modify the disease [3]. AD is pathologically characterized by the neurofibrillary tangles assembled from hyper-phosphorylated tau protein and the accumulation of amyloid- β peptides ($A\beta$) that form plaques in the extracellular region [4]. Apart from these two most recognized pathologies, there exist other characteristics including neuronal synaptic dysfunction, oxidative stress, and vascular issues that contribute to AD [5–7].

Current anti-AD drug developments mainly focus on strategies against $A\beta$ or tau, often through their relevant intermedia mechanisms as listed above [8–10]. The promising “disease-modifying” drugs poised at Phase 3 trials (21 agents) in 2022 were reviewed in a special report, in which the most represented mechanism was $A\beta$ (6), followed by synaptic plasticity (4), oxidative stress (3), metabolism (3), tau (1), etc. [10]. Despite the substantial ongoing clinical and experimental studies, researchers tend to acknowledge a single cure for AD would unlikely be found [11–13]. In such cases of complex diseases, signal networks could be the cause, and the anterior ‘one disease-one target-one drug’ dogma needs to be reconsidered [14].

Traditional Chinese Medicine (TCM) prescription is a time-proven medical discipline emphasizing the synergic effects of herbal combinations with empirical evidence [15,16]. In China, TCM prescriptions have been extensively implemented into the medical management for AD due to their nature of multi-targeting and low side effects [17,18]. Erzhi Wan (EZW), a classic TCM formula, is reputed for its efficacy on “liver and kidney yin deficiency” syndrome, while such syndrome underlies aging-related cognition impairment and memory loss in TCM theory [19,20]. The formula is composed of two herbs, namely Nvzhenzi (NZZ, *Ligustrum lucidum* Ait.) and Mohanlian (MHL, *Eclipta prostrata* L.). Previous *in-vivo* and *in-vitro* studies have demonstrated that NZZ and MHL function in neuroprotective activities potentially via anti-oxidative stress effects [21,22]. Moreover, pharmacological studies have shown that EZW (0.75 and 1.5 g/kg/day for 14 days) can improve the cognitive ability of AD model rats [23]. Additionally, EZW (0.7 and 1.4 g/kg/day for 12 weeks) ameliorated lipid metabolism and oxidative stress in ovariectomized ApoE-deficient mice [24]. Given that EZW could be a novel complementary medication against AD, the underlying mechanisms need to be systematically investigated.

Network pharmacology offers a system biology-based strategy aiming to target causal mechanisms through biological network modulation [14]. The indigenous advantage of network pharmacology in addressing complex diseases resides in its multi-target signaling attribute aligning well with the synergic principles of TCM prescription [25]. The human microarray platform is a promising tool for the detection of genetic alterations along with their distributions in organs and tissue for many diseases [26]. In our case, we examined the correlation between the putative targets of EZW and AD pathology by analyzing GEO datasets derived from clinical practice, enhancing the reliability of our findings. Furthermore, computational methods such as omics analysis, molecular docking, and molecular dynamics (MD) simulation, have been proposed for high-throughput drug discovery with efficacy and thus could accelerate the translation of research findings to clinical applications [27–29]. Therefore, our study explored the potential and the underlying mechanisms of EZW as an anti-AD medication through a combination of network pharmacology, bioinformatics analysis of GEO datasets, and *in silico* study of molecular docking and MD simulation.

In our study, we utilized network pharmacology to predict the active components, potential targets, and enrichment pathways of EZW against AD. Bioinformatics analysis can derive the core targets related to $A\beta$ and tau pathology, followed by the validation of binding affinity with molecular docking and MD simulation approaches. Through a comprehensive literature research, we elucidated the effects of EZW on AD, particularly in $A\beta$ and tau pathology, oxidative stress, synaptic plasticity, and neuronal death, mediated by the p53/PI3K/Akt signaling pathway. Eventually, we identified acacetin, β -sitosterol, and 3-*O*-acetyldammareneediol-II as the active components of EZW, which potentially exerted therapeutic effects on AD through interacting with AR, CASP8, POLB, and PREP. A schematic overview of our study protocol is shown in Fig. 1.

2. Methods

2.1. Collection of the active components and ADME evaluation

The active components of EZW were achieved from the Traditional Chinese Medicine System Pharmacology Database and Analysis Platform (TCMSP, <https://old.tcm-sp-e.com/tcm-sp.php> (accessed on October 6, 2022)) [30], followed by a pre-screening with the criteria as follows: oral bioavailability (OB) $\geq 30\%$ [31], drug-likeness (DL) ≥ 0.18 [32] and Caco-2 ≥ -0.4 [33], along with the assessment of blood-brain barrier (BBB) permeability [34]. The properties of the obtained components were cross-checked using the SwissADME website (<http://www.swissadme.ch/> (accessed on October 6, 2022)) for the evaluation of the absorption, distribution, metabolism, and excretion (ADME) parameters, pharmacokinetic properties, and drug-like nature, especially the violation of Lipinski's rule of five [35].

2.2. Target fishing of the EZW active components against AD

The common names and the canonical SMILES strings of the active components were retrieved from the PubChem database (<https://pubchem.ncbi.nlm.nih.gov/> (accessed on October 6, 2022)). To predict the targets of these components, we utilized a combination of sources: the SwissTargetPrediction website (<http://www.swisstargetprediction.ch/> (accessed on October 6, 2022)) [36], the PharmMapper server (<https://www.lilab-ecust.cn/pharmmapper/> (accessed on January 16, 2024)) [37], and the TCMbank (<https://tcm-bank.cn/> (accessed on January 16, 2024)) [38]. The specific criteria for each method were targets with predicted probability above zero for SwissTargetPrediction, the top 300 targets based on fit scores that matched with the druggable pharmacophore

models in pharmMapper, and targets mapped with active components by TCMbank.

Disease targets were collected from Genecards (<https://www.genecards.org/> (accessed on October 6, 2022)) [39], NCBI (<https://www.ncbi.nlm.nih.gov/> (accessed on October 6, 2022)) [40], and OMIM (<https://www.omim.org/> (accessed on October 6, 2022)) [41], taking “Alzheimer’s Disease” as the keyword, while the duplications were removed using Microsoft Excel software.

We further assessed the intersection targets of EZW and AD via the EVenn online tool (<http://www.ehbio.com/test/venn/>). The common targets represented the putative targets of EZW against AD.

2.3. Drawing of “anti-AD Targets-Components-Herbs” network

Cytoscape 3.9.1 software was employed to build the “anti-AD Targets-Components-Herbs” network for the visualization of the interconnections among herbs, their components, and the corresponding targets [42].

2.4. Construction of PPI network and clustering analyses

Protein-protein interaction (PPI) information was obtained from the STRING website (<https://string-db.org/> (accessed on January 16, 2024)) [43]. The organism criterion was set to Homo sapiens, and the interactions that conformed to the minimum required score (≥ 0.4) were considered significant. In the network, the node represented individual target proteins, while their connections were manifested by edges. The node degrees and the topological information of the PPI network were identified by built-in modules of Cytoscape 3.9.1 software. Isolated targets were removed before the visualization.

We utilized the Molecular Complex Detection (MCODE) plugin to detect densely connected molecular complexes in the PPI network [44]. The parameters for MCODE were specified as follows: degree cutoff = 2, node score cutoff = 0.2, k-core = 2, and max depth = 100.

2.5. GO and KEGG pathway enrichment analyses

Selected targets were evaluated by Gene Ontology (GO) and Kyoto Encyclopedia of Genes and Genomes (KEGG) enrichment analyses utilizing “clusterProfiler” and “org.Hs.eg.db” R packages [45]. The achieved datasets were subsequently uploaded to Sangerbox (<http://sangerbox.com/>) to visualize the results in the ascending order of log P values.

2.6. GEO genetic difference analysis of AD pathology related EZW targets

Potential targets of EZW against AD were input in Alzdata (<http://www.alzdata.org/> (accessed on January 18, 2024)) database for the calculation of convergent functional genomic (CFG) ranks to prioritize AD candidate genes [46]. One CFG score was added if the target met any following prerequisite: (1) governed by AD genetic variants; (2) exhibited physical interactions with APP, PSEN1, PSEN2, APOE, or MAPT; (3) differentially expressed in AD mouse models; (4) significantly correlated with A β or tau pathways. Only the targets correlated (P-value < 0.05) with AD pathology (A β and tau) were considered for the further Gene Expression Omnibus (GEO) gene differential analysis. Normalized expression profiles of screened targets were established from cross-platform GEO datasets of clinical AD case samples by the “Differential Expression” module of Alzdata. Accordingly, the defined differentially expressed genes (DEGs) of AD patients in the combined GEO dataset follow the criteria of log₂ fold change greater than 0.1 ($|\log_{2}FC| > 0.1$) and a false discovery rate smaller than 0.05 (FDR < 0.05). The results were subjected to R software, GraphPad Prism, and SangerBox for graphical presentations.

2.7. Molecular docking and binding pockets prediction

Molecular docking is a computational method frequently applied in drug discovery for its capability to predict the conceivable binding modes along with the affinity of protein-ligand complexes [47]. In our studies, the dockings were carried out between the core targets related to AD pathology and their corresponding active components. The procedure was as follows [48]:

(1) Docking preparation: The protein crystal structures were obtained from Protein Data Bank (PDB, <https://www.rcsb.org/> (accessed on October 24, 2022)) [49], and any missing residues were filled in using the SWISS-MODEL (<https://swissmodel.expasy.org/>) automated homology modeling server [50]. Briefly, the FASTA formats of the protein sequences were achieved from NCBI and cross-checked in the UniProt database (<https://www.uniprot.org/>). The sequences were then uploaded to the SWISS-MODEL server to build the models with previously determined templates. After the removal of water and ligands with PyMOL software, the proteins were configured in AutoDockTool 1.5.7 by adding hydrogen atoms, computing Gasteiger charges, and assigning Autodock4 (AD4) type to each macromolecule atom.

- (2) Ligand preparation: The molecular structures of active components were collected from the TCMSP database and input in the AutoDockTool 1.5.7 as ligands. In the torsion tree module, choose root, detect root, show root expansion, and choose torsion were successively conducted to set the parameters.
- (3) Defining docking parameters: The configured proteins and ligands were input in the Macromolecule and the Set Map Type modules, respectively. A tunable grid box was constructed for each target protein to define the molecular docking range. The grid box sizes were adjusted until the proteins were fully covered to ensure a blind docking process.

- (4) Molecular docking and visualization: Autodock 4.2.6 was applied for the molecular docking as well as the assessment of the binding affinity. Dockings were implemented by inputting the configured proteins and ligands in the Macromolecule and the Ligand modules, respectively. The Genetic Algorithm was adopted to generate 50 docking poses for each ligand. The docking parameters were set as default. Typically, binding energy less than -5 kcal/mol indicated favorable binding affinity [51].

Subsequently, the achieved conformations underwent automatic pocket detection and druggability assessment using the DoGSiteScorer server (<https://proteins.plus/> (accessed on February 1, 2024)). Ligand interactions with protein pockets scoring higher than 0.5 on the druggability scale were selected for further evaluation [52]. BIOVIA Discovery Studio Visualizer 2019 and PyMOL were utilized for the visualization of interaction types and the binding mode between ligands and proteins.

2.8. Molecular dynamics simulation verification

The optimal conformations of the protein-ligand complexes obtained from docking results were sequentially subjected to the molecular dynamics (MD) simulation approach to evaluate the binding stability utilizing GROMACS 2020.06 software [53]. MD simulation can predict the trajectory of atoms and molecules under physical conditions mimicking the body environment. We adopted the AMBER99SB-ILDN/GAFF force field for each simulation system, implemented by Sobtop (<http://sobereva.com/soft/Sobtop/> (accessed on January 19, 2024)). The initial system was constructed in a dodecahedron box with a 1.2 nm layer between the protein surface and the edge of the box, populated by the TIP3P water model. Each system was neutralized by adding appropriate amounts of Na^+ and Cl^- counter ions. Prior to the MD simulation, energy minimization was executed with the steepest descent algorithm. Then, the canonical (NVT) and isothermal-isobaric (NPT) ensemble were implemented to equilibrate the system for 100 ps. The state-balanced system was configured to maintain a constant temperature of 310 K and standard 1.0 bar pressure, along with the periodic boundary condition. Finally, the system underwent a 100 ns MD simulation to assess complex stability.

For the analysis of the MD simulation trajectory, we calculated the Root mean square deviation (RMSD), the Radius of gyration (ROG) value, the Root mean square fluctuation (RMSF), and the Solvent-accessible surface area (SASA) using GROMACS tools including *gmx rms*, *gmx gyrate*, *gmx rmsf*, and *gmx sasa*, respectively. The number of hydrogen bonds was determined using *gmx hbond*. The hydrogen bond coverage across the simulation period was estimated utilizing the *gmx hbdat* bash script (http://github.com/Jerkwin/gmxttools/tree/master/gmx_hbdat). Principal component analysis (PCA) of the last 50 ns MD trajectory and free energy landscape (FEL) analysis were performed using *gmx covar* and *gmx sham*, respectively.

To estimate the binding free energy (BFE), the molecular mechanics/Poisson-Boltzmann surface area (MM/PBSA) strategy was conducted via *gmx mmpbsa* bash script (http://github.com/Jerkwin/gmxttools/tree/master/gmx_mmpbsa). Generally, the BFE of ligand and protein in an aqueous solvent (ΔG_{bind}) can be expressed as:

$$\Delta G_{bind} = G_{Complex} - (G_{Protein} + G_{Ligand}) \quad (1)$$

and each G term is given by

$$G_i = E_{MM} + G_{solvent} - TS \quad (2)$$

Therefore, ΔG_{bind} can be calculated as:

$$\Delta G_{bind} = \Delta H - T\Delta S \quad (3)$$

where ΔH can be further decomposed as:

$$\Delta H = \Delta E_{MM} + \Delta G_{solvent} \quad (4)$$

$$\Delta E_{MM} = \Delta E_{coul} + \Delta E_{vdw} \quad (5)$$

$$\Delta G_{solvent} = \Delta G_{PB} + \Delta G_{SA} \quad (6)$$

In the above equations, terms represented as follows: ΔE_{MM} : change in gas-phase molecular mechanics energy; $\Delta G_{solvent}$: change in solvent-free energy; $-T\Delta S$: change in conformational entropy upon ligand binding; ΔE_{coul} : change in Coulomb interaction energy; ΔE_{vdw} : change in van der Waals energy; ΔG_{PB} : change in polar solvation energy; ΔG_{SA} : change in non-polar solvation energy. The entropy term ($-T\Delta S$) was calculated by the interaction entropy (IE) method as follows [54]:

$$-T\Delta S = k_B T \ln \langle e^{(\Delta E_{MM(i)} - \langle \Delta E_{MM} \rangle) / k_B T} \rangle \quad (7)$$

where k_B is the Boltzmann constant. The calculations were made with snapshots at 1 ns interval for the last 50 ns trajectory, resulting in a total of 50 frames to observe the evolution across the MD period.

3. Results

3.1. Screening the active components of EZW

In total, 167 chemical compounds from the two herbs in EZW were collected from the TCMSP database. After a stepwise screening process, we identified 17 active components under the criterion conditions of oral availability, intestinal permeability, and drug-likeness. The chemical structures of these filtered active components are provided in [Supplementary Fig. S1](#). Remarkably, all the active components satisfy Lipinski's rule of five, since no more than one violation is observed [55,56]. The pharmacological information of these components is listed in [Table 1](#).

3.2. Preliminary exploration of holistic effects of EZW against AD

Emerging evidence underscores a significant interplay between peripheral immunity and the central nervous system in AD [57,58]. Several drugs currently under clinical investigation have demonstrated efficacy against AD by mitigating peripheral inflammation [59]. For instance, semaglutide, a non-BBB permeable drug poised at Phase 3 trial, has shown promise in ameliorating cognition in the 3xTg mouse model of AD [60,61]. To ensure a comprehensive evaluation of EZW, we initially considered all the identified active components. After the deduplication, we obtained 586 EZW-related targets from online tools corresponding to 17 active components. Additionally, 2260 AD-related targets were retrieved from Genecards, NCBI, and OMIM databases ([Supplementary Table S1](#)). A Venn diagram was then utilized to manifest the intersections (250 common targets) between EZW and AD ([Fig. 2A](#)). To achieve a preliminary understanding of the molecular mechanism in EZW's action against AD, we performed a KEGG enrichment analysis on the intersected targets. The top-ranked enriched KEGG pathways in five categories are displayed in the ascending order of adjusted P-value ([Fig. 2B](#)). These pathways include lipid and atherosclerosis (hsa05417), PI3K-Akt signaling pathway (hsa04151), Apoptosis (hsa04210), IL-17 signaling pathway (hsa04657), and Arachidonic acid metabolism (hsa00590). To further interpret the result of the KEGG enrichment analysis, intersections among the top two enriched KEGG terms in each category were extracted alongside Alzheimer disease (hsa05010), and depicted in an UpsetR plot ([Fig. 2C](#)). The results reveal that Alzheimer disease (hsa05010) exhibits the most exclusive genes and shares common targets with other KEGG terms except for Tryptophan metabolism (hsa00380). Given that Alzheimer disease (hsa05010) is a defined pathway that mainly correlates with A β and tau pathology, we further concentrated on the mechanism of EZW against AD pathology in brain regions as such.

3.3. Evaluating the synergic effects of active components with BBB permeability

To assess the effects of EZW on AD pathology within brain regions, we extracted the active components that exhibit BBB permeability, along with their associated targets for subsequent investigations. These components include acacetin, β -sitosterol, pratensein, and 3-O-acetyldammarenediol-II, while the corresponding targets are listed in [Table 2](#). It is noteworthy that these four components display satisfactory metabolism properties, with a drug half-life exceeding 4 h ([Table 1](#)) [62]. Afterward, we constructed an "anti-AD Targets-Components-Herbs" network, resulting in 194 connections between four active components and 140 potential targets ([Fig. 3](#)). Among these components, acacetin (degree = 76) exhibits the highest degree of connectivity, followed by β -sitosterol (degree = 44), pratensein (degree = 43), and 3-O-acetyldammarenediol-II (degree = 31). Meanwhile, we notice the average of the target degree is 1.38, indicating synergic effects among active components in targeting AD. These reflect the multi-component and

Table 1
Pharmacological properties of the active components in EZW.

MOL Id	Molecular name	MW	OB%	Caco-2	DL	HL (Hour)	Lipinski's rules violation	BBB permeability
MOL001689	acacetin	284.28	34.97	0.67	0.24	17.25	0	moderate
MOL003398	pratensein	299.27	39.06	0.39	0.28	17.13	0	moderate
MOL000358	beta-sitosterol	414.79	36.91	1.32	0.75	5.36	0	strong
MOL005169	3-O-Acetyldammarenediol-II	486.86	40.23	1.09	0.82	9.14	1	strong
MOL000006	luteolin	286.25	36.16	0.19	0.25	15.94	0	No
MOL000098	quercetin	302.25	46.43	0.05	0.28	14.40	0	No
MOL000422	kaempferol	286.25	41.88	0.26	0.24	14.74	0	No
MOL002975	butin	272.27	69.94	0.3	0.21	16.80	0	No
MOL003378	1,3,8,9-tetrahydroxybenzofurano [3,2-c] chromen-6-one	300.23	33.94	0.01	0.43	9.62	0	No
MOL003389	3'-O-Methylorobol	300.28	57.41	0.45	0.27	17.31	0	No
MOL003402	demethylwedelolactone	302.25	72.13	0.04	0.43	9.17	0	No
MOL003404	wedelolactone	314.26	49.6	0.32	0.48	9.61	0	No
MOL004576	taxifolin	304.27	57.84	-0.23	0.27	14.41	0	No
MOL005147	lucidumoside D_qt	406.47	54.41	-0.04	0.47	5.83	0	No
MOL005190	eriodictyol	288.27	71.79	0.17	0.24	15.81	0	No
MOL005195	syringaresinol diglucoside_qt	450.48	83.12	0.33	0.8	3.29	0	No
MOL005209	lucidusculine	401.60	30.11	0.16	0.75	10.55	0	No

MW: molecular weight; OB: oral bioavailability; DL: drug likeness; HL: Drug half-life ($t_{1/2}$); BBB: blood-brain barrier.

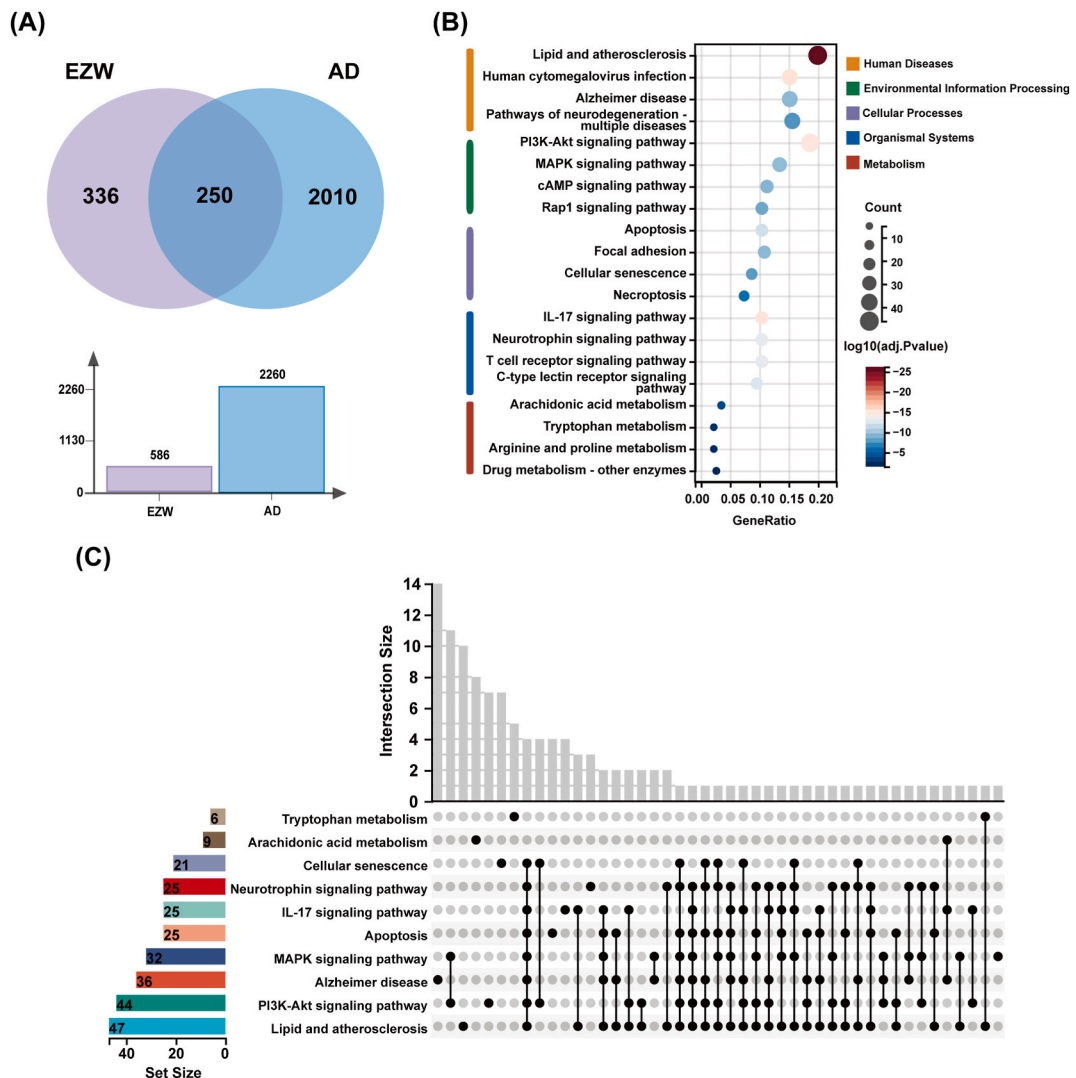


Fig. 2. Initial exploration of the potential efficacy that Erzhi Wan (EZW) exhibited against Alzheimer's disease (AD). (A) Venn diagram displaying the common targets of EZW and AD. (B) Bubble diagram of the KEGG enrichment pathways in the ascending order of adjusted P-value per category. (C) UpsetR plot displaying the intersections of KEGG enrichment sets.

multi-target nature of TCM, highlighting the intricate interactions between the potential targets that warrant further investigation.

3.4. PPI network analysis of the potential targets

Subsequently, we constructed a PPI network comprising 140 potential targets (Fig. 4). The PPI network manifests the interactions among the targets, offering comprehensive visions regarding the disease pathway network [14]. As shown in Fig. 4A, the PPI network contains 140 nodes and 1355 undirected edges. The average node degree and cluster coefficient of the PPI network are 19.36 and 0.536 respectively. The node sizes reflect the degree values, with the top ten targets highlighted based on their ranked degree. The topological information of these ten targets is listed in Table 3, including the degree value, betweenness centrality (BC), and closeness centrality (CC). MCODE plugin was applied for the cluster analysis, by which 8 clusters were identified. Table 4 presents detailed information on these MCODE clusters, and the three top-scored clusters are shown individually in Fig. 4B–D, along with the most relevant pathway per category excluding the human diseases. The seed nodes of clusters 1 and 3 were identified as AR and CYP19A1, respectively, while the seed node was not assigned to cluster 2 by the MCODE algorithm. As shown in Fig. 4B and C, cluster 1 is implicated with the p53 signaling pathway, PI3K-Akt signaling pathway, and IL-17 signaling pathway, while cluster 2 participates in Gap junction, Neuroactive ligand-receptor interaction, and Serotonergic synapse. These together indicate that the active components might exert therapeutic effects against AD pathology by modulating the network of potential targets.

Table 2
Potential targets of the active components of EZW with BBB permeability.

No.	Target	No.	Target	No.	Target	No.	Target
1	ABAT	37	CYP19A1	73	LTF	108	PREP
2	ABCB1	38	CYP1A1	74	MAOA	109	PRKCQ
3	ACHE	39	DAPK1	75	MAOB	110	PRPS1
4	ADAM17	40	DDP4	76	MAPK14	111	PRSS1
5	ADORA1	41	DRD2	77	MIF	112	PTGER2
6	ADORA2A	42	DRD4	78	MMP12	113	PTGES
7	ADRB2	43	DSG2	79	MMP13	114	PTGS1
8	AHR	44	EGFR	80	MMP2	115	PTGS2
9	ALDH2	45	ESR1	81	MMP3	116	PTK2
10	ALK	46	ESR2	82	MMP9	117	PTPN1
11	ALOX12	47	F10	83	MPO	118	PYGL
12	ALOX15	48	F2	84	MS4A1	119	RAB7A
13	ALOX5	49	FASLG	85	MTRR	120	RELA
14	APP	50	FKBP4	86	MYBPC3	121	RORA
15	AR	51	FLT3	87	NAE1	122	S100A8
16	ARG1	52	FOLH1	88	NCF1	123	SERPING1
17	AVPR2	53	G6PD	89	NOS2	124	SHBG
18	B2M	54	GART	90	NR1H2	125	SIGMAR1
19	BACE1	55	GCDH	91	NR1H3	126	SLC6A2
20	BAX	56	GLO1	92	NR3C1	127	SLC6A4
21	BCHE	57	GLRA1	93	OGT	128	SNCA
22	BCL2	58	GSK3B	94	OPRD1	129	SOD2
23	CA2	59	GSTT1	95	PARP1	130	SRC
24	CALM1	60	HMGCR	96	PCSK9	131	SYK
25	CAMK4	61	HSD11B1	97	PIK3R1	132	TERT
26	CASP3	62	HSP90AA1	98	PLA2G2A	133	THRB
27	CASP8	63	HTR2A	99	PLAT	134	TLR9
28	CCNA2	64	HTR2C	100	PLAU	135	TP53
29	CDK1	65	IDE	101	PLG	136	TTR
30	CDK5R1	66	IGF1R	102	POLB	137	TYR
31	CDKN1A	67	IGFBP2	103	PON1	138	VDR
32	CFTR	68	IGFBP3	104	POT1	139	WARS1
33	CHEK1	69	IGFBP6	105	PPARA	140	XDH
34	CHRM2	70	IL2	106	PPARD		
35	CSNK2A1	71	KDR	107	PPARG		
36	CYP17A1	72	LCK	108	PPP2R1A		

3.5. Functional pathway analysis of the potential targets in AD treatment

To further explore the therapeutic mechanisms of active components against AD pathology, KEGG pathway analysis was carried out to annotate the functions of these 140 potential targets (Fig. 5A). The enriched signaling pathways mainly include Alzheimer disease (hsa05010), PI3K-Akt signaling pathway (hsa04151), P53 signaling pathway (hsa04115), Serotonergic synapse (hsa04726), and Arachidonic acid metabolism (hsa00590), indicating these pathways would play a predominant role in conferring efficacy of EZW against AD.

Similarly, GO enrichment analysis was conducted particularly in terms of biological process (BP), cellular components (CC), and molecular function (MF) to reveal the representative functions of the targets. Accordingly, we obtained 2024 BP, 123 CC, and 203 MF terms and depicted the top 10 enrichments in each group in Fig. 5B. The result shows that the significantly enriched BP terms include response to oxygen level (GO:0070482), neuron apoptotic process (GO:0051402), and regulation of inflammatory response (GO:0050727).

3.6. Derivation of core targets that correlated with A β and tau pathology through bioinformatics analysis

To determine the relationship between the active components and the AD pathology, we uploaded the potential targets to the AlzData database for the mining of their correlations with A β and tau protein. Consequently, 41 out of 140 targets were identified, showing significant correlations with AD pathology in A β and tau line AD mouse models. Among these, 15, 8, and 18 targets map to the A β , tau, and A β and tau, respectively. The detailed information on these targets is listed in Supplementary Table S2. Additionally, the CFG points of these targets were calculated by integrating AD-relevant evidence (Fig. 6A). Typically, the prioritizing method indicates that NR1H3, AR, MMP2, CHRM2, RORA, LCK, RELA, PCSK9, B2M, FKBP4, and BACE1 exhibit high-level AD relations (CFG \geq 4) compared to the others.

To further validate the implications of these targets, we utilized the normalized cross-platform GEO datasets of clinical samples. Differentially expressed genes (DEGs) were examined in four brain regions—hippocampus, entorhinal cortex (EC), frontal cortex (FC), and temporal cortex (TC)—between control and AD patient groups. Accordingly, 41 targets related to A β and tau pathological events as well as APP itself were analyzed utilizing the embedded “Differential Expression” module in the Alzdata database. The expression

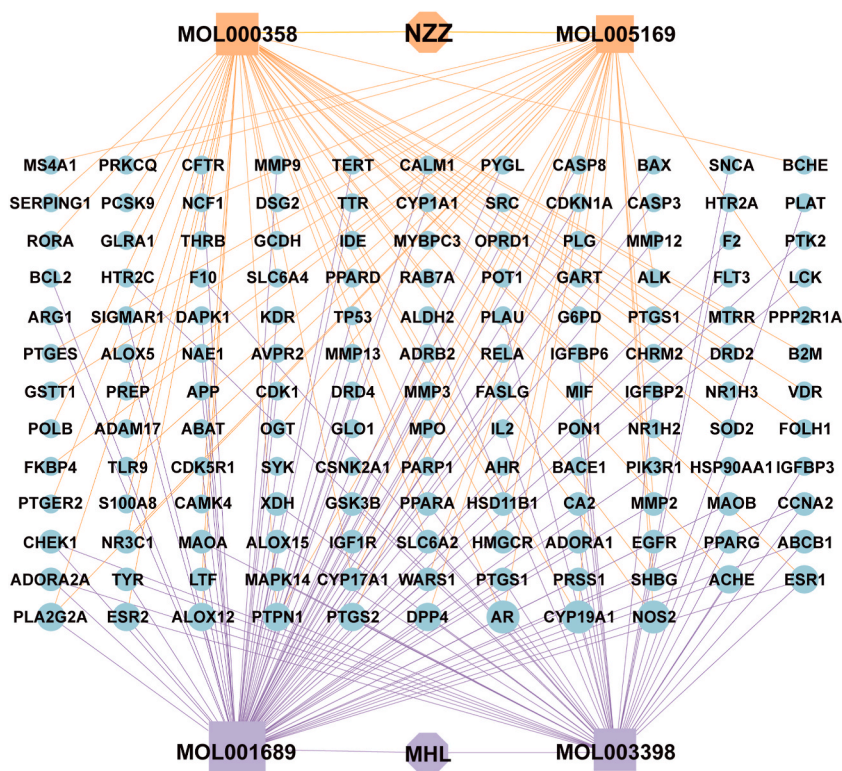


Fig. 3. The anti-AD Targets-Component-Herb network. The octagons represent herbs. The squares and the circles represent the active components and their corresponding intersected genes respectively, while the node sizes are proportional to the degrees independently between groups.

profiles of these targets were integrated into a volcano plot (Fig. 6B). The details of the expression profile regarding the hippocampus are listed in Table 5, while the rest are available in Supplementary Table S3. The results show that 25 targets are differentially expressed in 4 brain regions yielding 45 variants, of which 17 are upregulated and 28 are downregulated. The normalized expression data of five DEGs in the hippocampus are displayed (Fig. 6C–G), while the remainder is presented in Supplementary Fig. S2 for clarity. The brain region distributions of the DEGs were consolidated into a Venn diagram (Fig. 6H). The results reveal that GLO1, POLB, PREP, and PPP2R1A are differentially expressed across all four brain regions, suggesting their potential predominant roles in therapy against AD pathology. Ultimately, an interactive network was constructed for the direct visualization of the associations among DEGs, active components, and herbs (Fig. 6I). The DEGs are intimately associated with A β and tau pathology in clinical practice and thus can be considered core targets for further validation.

3.7. Molecular docking and binding pocket prediction

To validate the interconnection between the 4 active components and 25 core targets, we performed an integrative approach of molecular docking and binding pocket prediction. 29 docking pairs from the previous findings were subjected to Autodock 4.2.6 for the assessment of binding affinity. The conformations with a favorable binding affinity were submitted to the DogSiteScorer server for the evaluation of ligand-binding pockets and their druggability. We collected the conformations that simultaneously met the criteria of molecular docking (binding energy < -5 kcal/mol) and DogSiteScorer (druggability score > 0.5). Since we generated 50 ligand poses for each protein, we selected those with the lowest binding energy as the optimal conformation per docking pair (Table 6). The interaction types and residues of the optimal conformations are listed in Supplementary Table S4. The heatmaps of the binding energies (kcal/mol) of all docking pairs are shown in Fig. 7A. As aforementioned A β and tau pathology correlated with hippocampus impairment and thus led to the loss of memory and cognition function, we selected the protein-ligand complexes comprised of core targets in the hippocampal region for further presentation and evaluation. Accordingly, five protein-ligand complex systems including AR (PDB ID: 5v8q)-acacetin, AR (PDB ID: 5v8q)-pratensein, CASP8 (PDB ID: 3h11)-acacetin, POLB (PDB ID: 1tv9)- β -sitosterol, and PREP (PDB ID: 3ddu)-3-O-acetyldammareniol-II were visualized in two- and three dimensions (2D and 3D) to make the docking results more intuitive (Fig. 7B–F).

Additionally, we conducted literature research (see discussion below) on these five docking pairs and utilized experimentally determined agonists or inhibitors as ligand controls to perform molecular dockings with the same parameters. The ligand controls and the corresponding binding affinity for AR, CASP8, POLB, and PREP are dihydrotestosterone (-6.73 kcal/mol), 2-(4-chlorophenyl)-N-(2-(1,2,3,6-tetrahydropyridazin-3-yl)ethyl)acetamide (-4.25 kcal/mol), dATP (-9.04 kcal/mol), and Z-Gly-Pro-PNA (-6.5 kcal/mol).

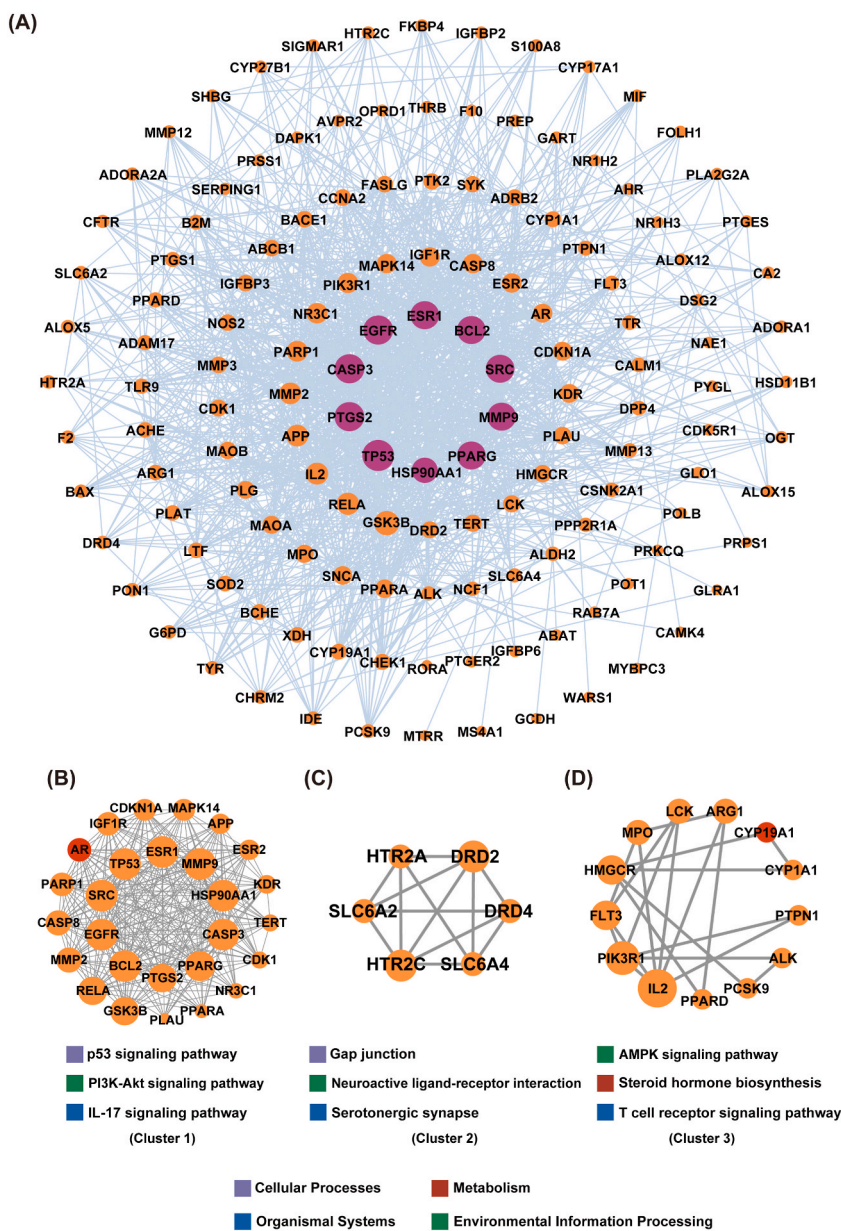


Fig. 4. The protein-protein interaction (PPI) analysis of the 140 potential targets. (A) PPI network. The nodes represent the target genes, while the node sizes are proportional to the node degrees. The top 10 targets ranked by degrees are highlighted in purple. (B–D) Clusters 1–3 identified by cluster analysis of MCODE. The seed nodes of individual cluster are displayed in red. Seed node was not assigned for cluster 2 by the MCODE algorithm. The KEGG enriched terms of each cluster are listed below the graphic. (For interpretation of the references to colour in this figure legend, the reader is referred to the Web version of this article.)

mol), respectively. The chemical structures of the ligand controls are shown in [Supplementary Fig. S3A](#), while detailed information on the comparison of ligand controls and active components can be found in [Supplementary Figs. S3B–E](#) and [Supplementary Table S5](#). The results confirm that active components can bind to the pockets with biological functions and verify the parameters of molecular docking.

3.8. MD simulation validation

Subsequently, these five docking systems were subjected to 100 ns MD simulation to test the binding stability in protein-ligand complexes. RMSD is a metric proposed for quantifying evolutions of atom coordinates in macromolecules against the initial frame. As shown in [Fig. 8A](#), the RMSD values of all five simulation systems are less than 1 nm, indicating a stable binding between protein and

Table 3
The topological information of top 10 targets in the PPI network.

Target	Degree	ClosenessCentrality	BetweennessCentrality
TP53	75	0.668	0.073
EGFR	68	0.647	0.064
CASP3	68	0.647	0.047
PTGS2	68	0.644	0.069
MMP9	64	0.626	0.043
SRC	64	0.629	0.069
BCL2	64	0.635	0.035
ESR1	64	0.632	0.062
PPARG	64	0.629	0.064
HSP90AA1	54	0.610	0.031

Table 4
The clustering information of MCODE analysis.

	Cluster 1	Cluster 2	Cluster 3	Cluster 4	Cluster 5	Cluster 6	Cluster 7	Cluster 8	
Node Count	29	6	13	3	3	3	3	3	
MCODE Score	23.357	5.2	3.333	3	3	3	3	3	
Seed node	AR		CYP19A1	IGFBP3	XDH	F10	PLA2G2A	NR1H2	
Lists of targets in clusters	MMP2 IGF1R PPARG PTGS2 RELA ESR2 MAPK14 CDKN1A CASP8 GSK3B PARP1 MMP9 APP TERT	CCNA2 CDK1 PLAU PPARA HSP90AA1 SRC NR3C1 KDR BCL2 CASP3 EGFR ESR1 TP53 PTK2	DRD2 HTR2C DRD4 SLC6A4 HTR2A SLC6A2	FLT3 PTPN1 IL2 HMGCR PPARD PIK3R1 ALK LCK MPO PCSK9 CYP1A1 ARG1	MMP3 PLG	MAOA ACHE	F2 SERPING1	ALOX15 PTGES	OGT NR1H3

No seed node was assigned to the cluster 2.

ligand. However, fluctuations are observed in CASP8-acacetin and POLB- β -sitosterol, implying the possibility of conformational change. Then, RMSF was measured to examine the deviation of individual atoms in macromolecules (Fig. 8B). Intense fluctuations are observed in CASP8 (PRO370-LEU385) and PREP (LYS196). Both protein regions are cleavage sites that can facilitate protein activities [63,64]. This might partially explain the inhibitory roles of active components. Furthermore, ROG was calculated as it can reveal the conformational state (protein folding) of macromolecules. As shown in Fig. 8C, the ROG value of the POLB- β -sitosterol complex slightly decreases during the simulation. To further interpret the results of ROG, SASA analysis was conducted (Fig. 8D). The tendency of SASA is consistent with ROG values. These together highlight the increasing compactness and structural stability of the POLB- β -sitosterol complex with lower exposure to water molecules, which potentially prohibits the bindings with other ligands [65].

MM/PBSA is a widely utilized strategy for the re-demonstration of the binding site and the binding strength between the protein and the ligand via the generated MD simulation trajectory without any additional efforts [66]. Combined with interaction entropy (IE), it is one of the most accurate estimation methods of binding free energy (BFE) in parallel with experiments. Herein, we calculated the BFEs of the five abovementioned ligand-protein complexes. The total BFEs of AR-acacetin, AR-pratensein, CASP8-acacetin, POLB- β -sitosterol, PREP-3-O-acetyldammarenediol-II are -64.31 ± 9.11 kJ/mol, -11.66 ± 12.32 kJ/mol, -57.40 ± 23.01 kJ/mol, -75.48 ± 13.12 kJ/mol, and -70.08 ± 13.77 kJ/mol, indicating favorable binding affinities except for AR-pratensein complex [67]. The high BFE of AR-pratensein results from the high IE and low MM/PBSA terms, implying the continuous deviation in conformations. The MM/PBSA results are listed in Table 7. To achieve the energy contribution of each amino acid, we conducted the per-residue decomposition analysis for the MM/PBSA energy across the last 50 ns MD trajectory. As shown in Fig. 8G, VAL684, VAL715, and MET745 contribute most to the binding energy of AR-acacetin. The MM/PBSA energies of these three residues are -5.272 kJ/mol, -4.789 kJ/mol, and -5.328 kJ/mol, respectively. For the AR-pratensein complex, the most contributed residues are PRO801 (-3.877 kJ/mol), LEU805 (-2.617 kJ/mol), and TRP751 (-2.235 kJ/mol). In the CASP8-acacetin complex, the most contributed residues are LEU381 (-5.269 kJ/mol), VAL406 (-6.788 kJ/mol), and MET463 (-4.768 kJ/mol). For the POLB- β -sitosterol complex, the most contributed residues are ILE33 (-8.337 kJ/mol), ARG40 (-4.755 kJ/mol), ASN279 (-4.096 kJ/mol), LYS280 (-8.488 kJ/mol), and ARG283 (-3.678 kJ/mol). In the case of PREP-3-O-acetyldammarenediol-II, the most contributed residues are ARG128 (-2.297 kJ/mol), ILE478 (-3.163 kJ/mol), GLY553 (-3.353 kJ/mol), VAL578 (-3.433 kJ/mol), and ALA682 (-4.707 kJ/mol). Collectively, active components bind to the pockets of AR, CASP8, and PREP-3-O-acetyldammarenediol-II mainly by VDW interactions, while the binding of POLB is favored by low polar solvation energy.

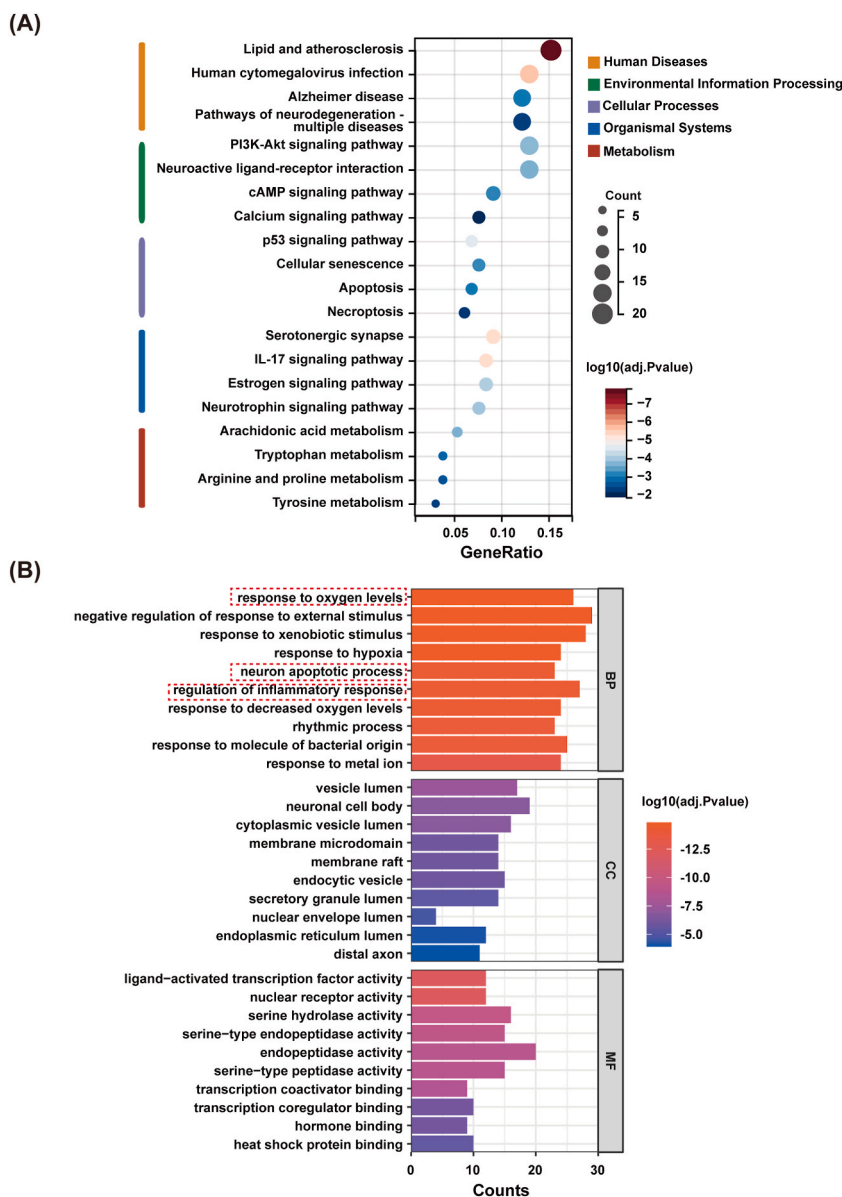


Fig. 5. The results of GO and KEGG enrichment analysis. (A) Bubble diagram of the top four KEGG enrichment pathways in the ascending order of logP values per category. (B) GO enrichment terms. Top 10 GO terms of biological process (BP), cellular components (CC), and molecular functions (MF) are displayed in the ascending order of logP values individually. The discussed BP terms are highlighted in red square. (For interpretation of the references to colour in this figure legend, the reader is referred to the Web version of this article.)

Hydrogen bonding analysis is important in featuring ligand-protein binding, as hydrogen bonds can steer the binding strength of small molecules. Through the built-in module of GROMACS software, we calculated the number and the population of hydrogen bonds between ligands and proteins in a time-dependent manner (Fig. 8E). The average number of hydrogen bonds in AR-acacetin, AR-pratensein, CASP8-acacetin, POLB- β -sitosterol, and PREP-3-O-acetyldammarenediol-II is 0.576, 0.769, 0.747, 0.125, and 0.040 per frame, respectively. Additionally, the hydrogen bond occupancy in each complex was estimated to reveal the key interacting residues. The occupancy results are listed as follows: AR-acacetin (PRO682: 32.2%; VAL685: 15.3%; LYS808: 9.7%); AR-pratensein (TRP751: 31.7%; ARG752: 16.3%; PRO801: 8.8%); CASP8-acacetin (ASN407: 21.5%; GLN465: 12.8%; ASN408: 11.5%); POLB- β -sitosterol (ARG283: 6.2%; LYS280: 3.4%; ASP: 1.8%); PREP-3-O-acetyldammarenediol-II (TYR471: 2.8%; CYS78: 0.4%; THR385: 0.3%). Apparently, AR and CASP8 complexes exhibit relatively stable hydrogen bonds that contribute to system stabilization, but not for POLB and PREP complexes.

To further analyze the interactions that contribute to stability between ligand and protein, the free energy landscapes (FELs) of the last 50 ns simulations were established by depicting the graphic between free energy and the first two principal components extracted

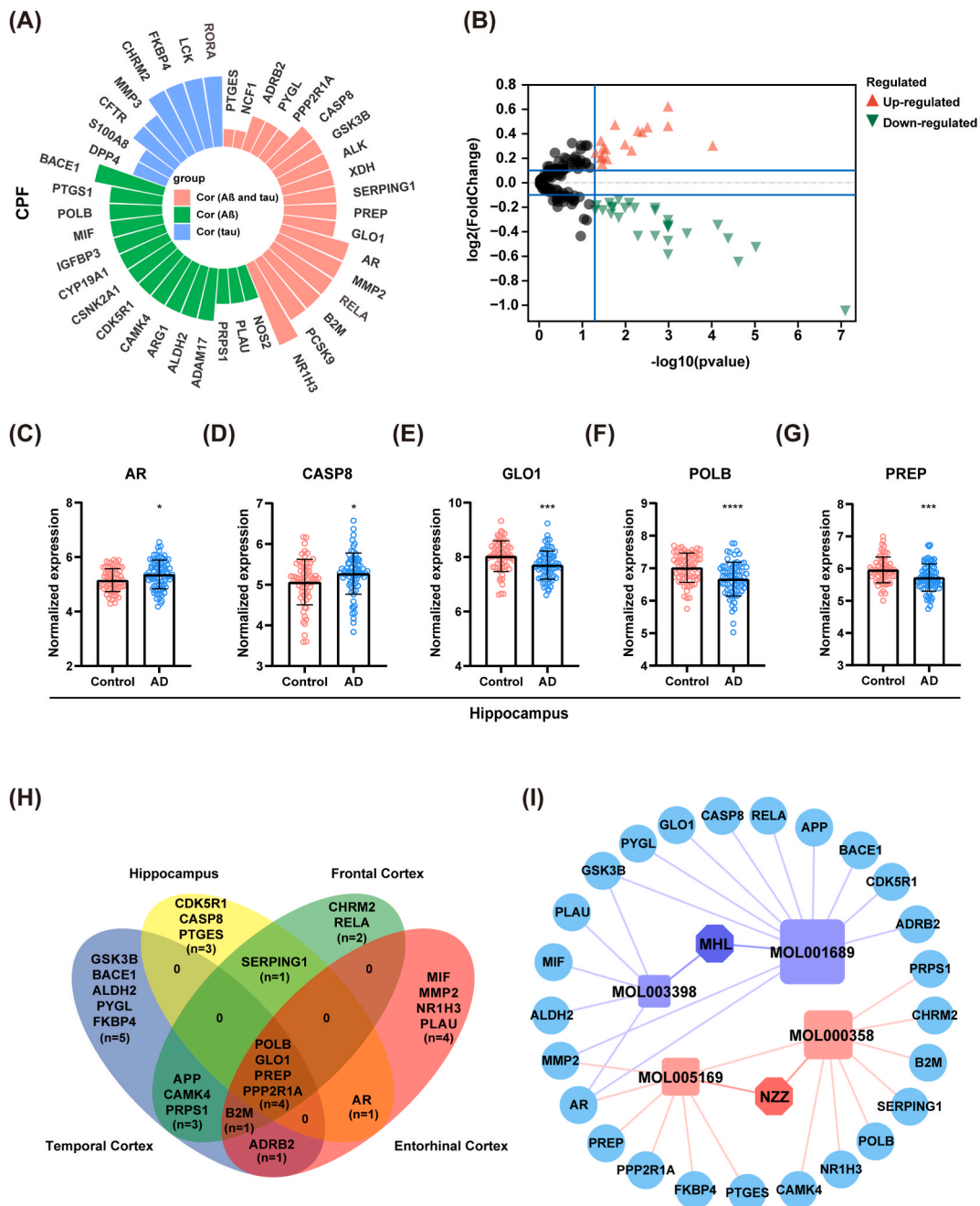


Fig. 6. Identification of the core targets correlating with Aβ and tau pathology based on bioinformatics analysis. (A) Circular bar plot displaying the targets that significantly correlated with Aβ and tau pathology. The bar sizes represent the convergent functional genomic (CFG) points. (B) The volcano plot showing the differentially expressed genes (DEGs) between control and Alzheimer's disease (AD) patients. (C–G) Results manifesting DEGs expression profiles from the GEO datasets. For the hippocampus, sample sizes are n = 66 and n = 74 in the control and AD patient group respectively. Results are shown in mean ± SD. (H) Venn diagram showing the targets distribution in 4 brain regions. (I) Interaction network displaying connections among DEGs, active components, and herbs. The circle, square, and the octagons are DEGs, active components, and herbs, respectively.

from principal component analysis (PCA). The FELs of POLB-β-sitosterol and PREP-3-O-acetyldammareniol-II complexes are displayed in Fig. 8H and I, while the rest are shown in Supplementary Fig. S4. The result suggests the interactions between β-sitosterol and POLB are mainly van der Waals, Carbon Hydrogen Bond, Pi-Alkyl, and Alkyl in minimum energy conformation. Combining with the results of the per-residue decomposition of MM/PBSA, ILE33 (-8.337 kJ/mol) and LYS280 (-8.488 kJ/mol) are reckoned to be the most contributed residues in complex stabilization through Pi-Alkyl and Alkyl interactions. In the case of PREP and 3-O-

Table 5
DEGs information based on analysis of GEO datasets.

Target	Brain region	log2 (Fold Change)	P-value	Expression pattern
SERPING1	HP	0.42	0.005	Upregulated
PTGES	HP	0.21	0.033	Upregulated
CASP8	HP	0.2	0.036	Upregulated
AR	HP	0.19	0.026	Upregulated
PREP	HP	-0.21	0.006	Downregulated
CDK5R1	HP	-0.23	0.033	Downregulated
GLO1	HP	-0.31	0.001	Downregulated
POLB	HP	-0.35	7.06E-05	Downregulated
PPP2R1A	HP	-0.37	0.001	Downregulated

HP: Hippocampus.

Table 6
Results of molecular docking and binding pocket detection.

PDB ID	MOL ID	Target	Affinity	Pocket volume (Å ³)	Ligand coverage (%)	Pocket coverage (%)	DrugScore
5v8q	MOL001689	AR	-6.49	906.69	96.97	25.82	0.837163
5v8q	MOL003398	AR	-5.23	906.69	88.24	20.6	0.837163
3h11	MOL001689	CASP8	-5.03	837.89	100	25.65	0.845761
1tv9	MOL000358	POLB	-5.52	437.25	70	46.02	0.806264
3ddu	MOL005169	PREP	-7.36	1001.93	61.8	16.17	0.797201
5d5a	MOL001689	ADRB2	-7.04	1653.18	100	18.14	0.806962
3n80	MOL003398	ALDH2	-6.6	369.51	52.94	26.23	0.613977
Q5IS80	MOL001689	APP	-5.4	7137.88	15.15	0.07	0.805306
				1058.86	51.52	9.85	0.801846
4dju	MOL001689	BACE1	-6.01	795.46	72.73	12.12	0.835135
5zk3	MOL000358	CHRM2	-6.41	1493.99	38.75	9.48	0.821135
				262.7	6.25	3.23	0.359991
4lay	MOL005169	FKBP4	-7.09	247.68	25.84	30.41	0.510928
1j1b	MOL001689	GSK3B	-6.04	868.42	100	33.69	0.80214
1ck7	MOL001689	MMP2	-6.66	391	57.58	37.1	0.604516
				308.32	18.18	4.81	0.678196
				245.38	3.03	0.27	0.382771
1ck7	MOL005169	MMP2	-6.15	125.87	35.96	39.78	0.604516
4nqa	MOL000358	NR1H3	-5.15	468.88	76.25	40.86	0.809455
2vnt	MOL003398	PLAU	-5.96	458.82	100	59.59	0.708267
115q	MOL001689	PYGL	-5.31	446.71	69.7	28.64	0.628925
				148.2	27.27	24.69	0.273259
1nfi	MOL001689	RELA	-5.24	307.22	69.7	42.31	0.532964

The affinity is provided in kcal/mol; The DrugScore ranges from 0 to 1.

acetyldammarenediol-II, the protein and ligand merely interact through van der Waals and Pi-Alkyl. However, the residues PHE80 (-0.02 kJ/mol), PHE89 (-0.309 kJ/mol), TRP340 (-0.052 kJ/mol), and TYR385 (-0.046 kJ/mol) that formed Pi-Alkyl with the ligand barely contribute to the MM/PBSA, indicating van der Waals interaction dominated the binding stability. Additionally, we observe the existence of two minimum energy basins in the AR-pratensein simulation system (Supplementary Fig. S4B). This might explain the high value of IE, as these two conformations can continuously transform into each other.

Collectively, we identified three active components including acacetin, β -sitosterol, and 3-O-acetyldammarenediol-II with therapeutic potentials against A β and tau pathology by targeting AR, CASP8, POLB, and PREP in the hippocampal region. We demonstrated the binding affinities, the binding pocket druggabilities, and the interactions between ligand and protein complexes.

4. Discussion

Alzheimer's disease (AD) is a neurodegeneration disorder that entails severe chronic consequences, leading to a costly burden [1]. Current anti-AD drug discovery is mainly addressed in aspects of A β and tau protein, often through their relevant mechanisms of oxidative stress, synaptic plasticity, etc. [10]. By its complicated and multifactorial nature, a causative treatment of a single cure for AD has yet to be enrolled [11–13]. As a complementary treatment, Traditional Chinese Medicine (TCM) has established its reputation for its multi-targeting and few side effects in treating diseases [16]. Erzhi wan (EZW) is a time-proven herbal prescription that contains Nvzhenzi (NZZ) and Mohanlian (MHL). In China, the applications of EZW in clinical practice mainly focus on treating aging-related diseases [19,20]. Additionally, modern pharmacological studies have shown that EZW (0.75 and 1.5 g/kg/day for 14 days) can ameliorate cognitive impairment in AD model rats [23]. However, its anti-AD mechanism has barely been illustrated. Herein, network pharmacology, bioinformatics, molecular docking, and molecular dynamics (MD) simulation were employed to analyze the spectrum relationship between active components of EZW with blood-brain barrier (BBB) permeability and their corresponding targets. As a

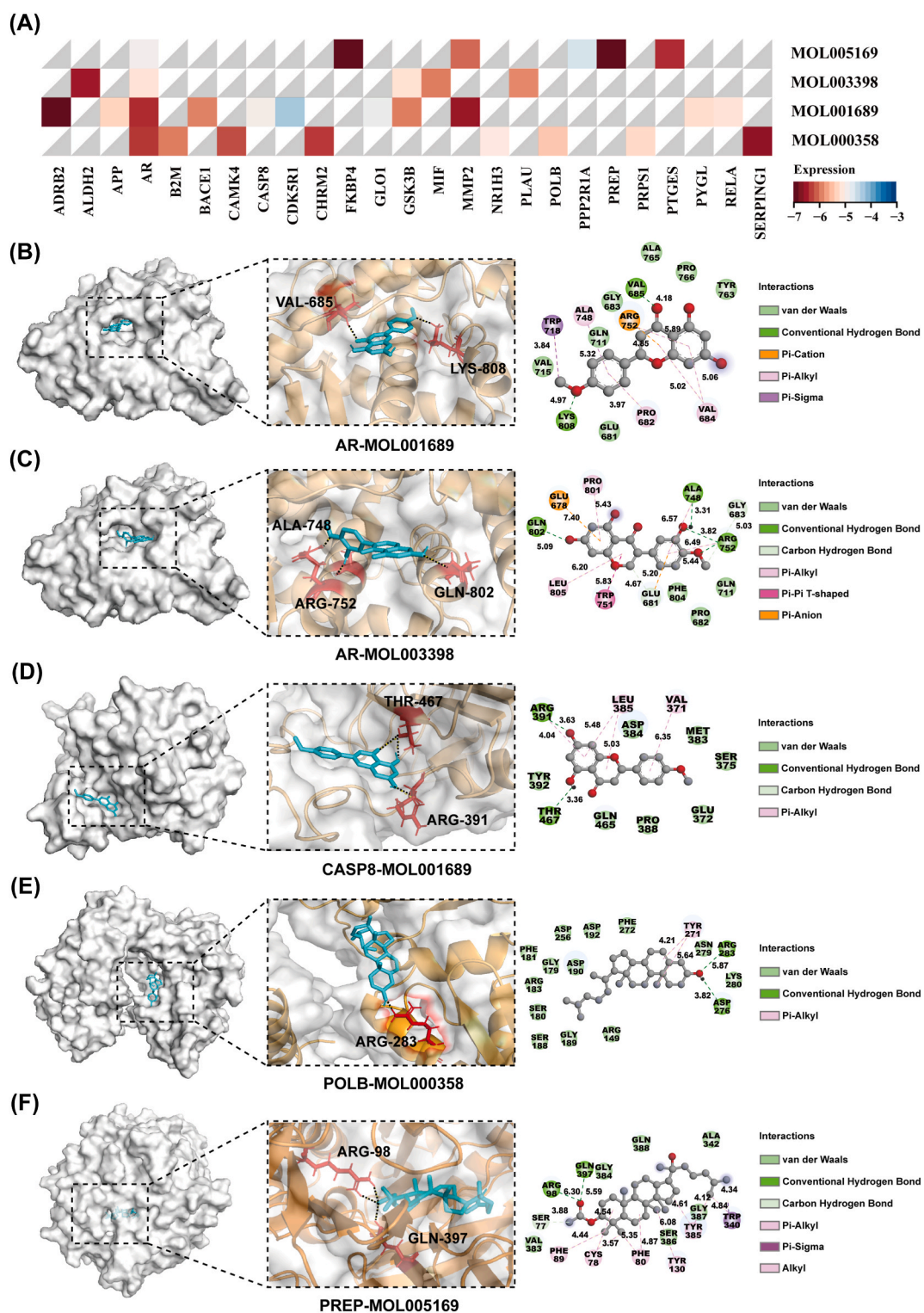


Fig. 7. Results of molecular docking. (A) Heatmap of the binding affinities (kcal/mol) between the active components and the core targets. (B–F) The graphic illustrations of the binding sites in two- and three dimensions (2D and 3D). (B) AR-acacetin. (C) AR-pratensein. (D) CASP8-acacetin. (E) POLB- β -sitosterol. (F) PREP-3-O-acetyldammarenediol-II. The binding pocket, zoomed-in views of hydrogen bonds in binding sites, ligand-interacted residues, and the corresponding interaction types are shown from left to right.

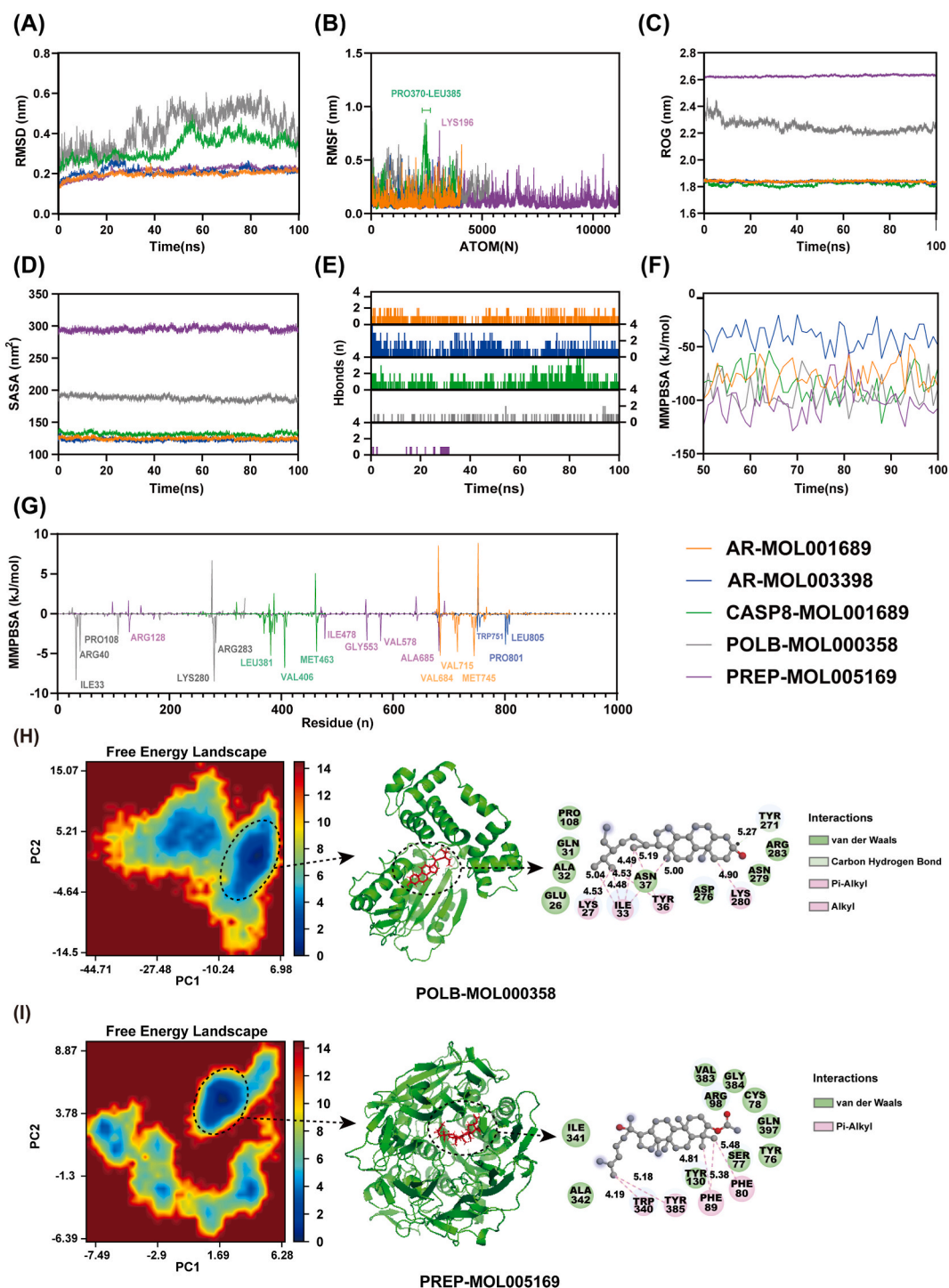


Fig. 8. Results of molecular dynamics (MD) simulation. (A) Root mean square deviation (RMSD). (B) Root mean square fluctuation (RMSF). Intensely fluctuated residues are highlighted. (C) Radius of gyration (ROG). (D) Solvent-accessible surface area (SASA). (E) Number of hydrogen bonds across the simulation period. (F) Evolution of molecular mechanics/Poisson-Boltzmann surface area (MM/PBSA) energies in last 50 ns simulations. (G) Per-residue decompositions of MM/PBSA energies. (H–I) The two-dimensional free energy landscape (FEL). The maximum and minimum energy basins are depicted in red and blue, respectively. The ligand-interacted residues and the corresponding interaction types of minimum energy conformations are illustrated in two- and three dimensions. (For interpretation of the references to colour in this figure legend, the reader is referred to the Web version of this article.)

Table 7
Calculated binding free energy via MM/PBSA strategy.

	AR-MOL001689	AR-MOL003398	CASP8-MOL001689	POLB-MOL000358	PREP-MOL005169
MM/PBSA (ΔH)	-77.48 ± 12.55	-40.71 ± 10.67	-83.92 ± 14.92	-93.58 ± 13.38	-102.28 ± 15.54
MM	-181.19 ± 10.52	-100.32 ± 19.29	-171.61 ± 24.06	-112.26 ± 12.46	-150.39 ± 12.78
PB	124.28 ± 9.46	72.81 ± 16.58	108.23 ± 24.11	39.29 ± 8.43	73.65 ± 14.92
SA	-20.56 ± 0.56	-13.21 ± 1.70	-20.54 ± 1.07	-20.61 ± 1.53	-25.54 ± 2.23
COU	-21.44 ± 7.44	-18.89 ± 9.71	-24.71 ± 13.76	-1.83 ± 2.14	-1.30 ± 4.20
VDW	-159.76 ± 8.57	-81.43 ± 15.38	-146.90 ± 16.49	-110.43 ± 12.60	-149.09 ± 12.12
- ΔS	13.34 ± 6.86	28.33 ± 10.67	25.82 ± 17.30	17.73 ± 5.01	10.16 ± 4.32
ΔG	-64.31 ± 9.11	-11.66 ± 12.32	-57.40 ± 23.01	-75.48 ± 6.15	-92.28 ± 7.83

The presented values were given in kJ/mol and with standard deviations (\pm SD). MM: gas-phase molecular mechanics energy.

PB: polar solvation energy; SA: non-polar solvation energy; COU: coulomb interaction energy; VDW: van der Waals energy.

- ΔS : change in conformational entropy.

result, we found the molecular mechanism of EZW treating AD intimately associated with the A β and tau pathology, oxidative stress, and synaptic plasticity, especially in the hippocampal region. Specifically, the in-depth bioinformatics and computational analyses demonstrate that acacetin, β -sitosterol, and 3-O-acetyldammarene diol-II are the main active components of EZW conferring efficacy against AD through targeting AR, CASP8, POLB, and PREP. Through literature research, we found these targets significantly involved in A β and tau pathology, oxidative stress, synaptic plasticity, and neuronal death.

Through database retrieval and a follow-up screening process, we eventually screened four active components of EZW with BBB permeability, along with their 140 corresponding anti-AD targets. Among these components, acacetin (100, 300, and 500 μ M) can reduce A β production via the inhibition of BACE-1 activity and APP synthesis [68]. In an amyloidogenic cleavage process, abnormal regulation of BACE-1 would cleave APP at the Asp¹ cleavage to produce a secreted form of carboxy-terminal fragments and reinforce the toxic A β production [69]. β -sitosterol is a member of phytosterols structurally similar to cholesterol. Evidence suggests that β -sitosterol can attenuate A β induced neuro-toxicity in the PC12 cell model by relieving oxidative stress [70]. Oxidative stress entails the imbalance between antioxidants and oxidants, that leads to the generation of reactive oxygen species (ROS). ROS can upregulate phosphorylated tau protein by inducing the malfunction of mitochondria in neurons and thus contribute to AD pathology [5,71]. Likewise, after oral administration for three weeks in the AD rat models, pratensein (10 and 20 mg/kg/day for 6 days) can improve cognitive deficits by reducing oxidative stress [72]. For the 3-O-acetyldammarene diol-II, no studies focus on its anti-AD effects currently. For the first time, our study demonstrates the potential of 3-O-acetyldammarene diol-II on AD therapies. As summarized, these four active components are proposed to treat AD in aspects of reducing abnormal A β and phosphorylated tau production and mitigating the neuro-toxicity through antagonizing oxidative stress.

The spectrum relationships of active components and the corresponding targets were manifested in a network diagram of “anti-AD Targets-Components-Herbs” that included four active components and 140 potential targets. Then, we constructed the PPI network to display the interconnections of these targets. Top 10 targets ranked by node degree are TP53, EGFR, CASP3, PTGS2, MMP9, SRC, BCL2, ESR1, PPARG, and HSP90AA1. Further interpretations of the PPI network rest on the MCODE, GO, and KEGG enrichment analysis. The results show that the targets are mainly enriched in Alzheimer disease (hsa05010), PI3K-Akt signaling pathway (hsa04151), P53 signaling pathway (hsa04115), Serotonergic synapse (hsa04726), and Arachidonic acid metabolism (hsa00590). Among these pathways, P53 and PI3K-Akt signaling pathways are associated with cluster 1 classified by the MCODE algorithm, while the Serotonergic synapse is implicated with cluster 2. In AD pathology, Src family kinase can enhance the BACE activity resulting in the A β production [73,74]. COX-2 (a key enzyme encoded by PTGS2) is involved in arachidonic acid conversion to prostaglandins, while the upregulation of the latter can induce A β deposition in the AD mice model [75]. Roles of MMPs in the brain can vary, wherein MMP9 can degrade A β plaque, while on the contrary, MMP2 is able to facilitate the A β plaque formation and tau aggregation [76]. TP53 and EGFR can be activated by A β oligomers, leading to A β -dependent memory loss. Their activations are often accompanied by the inhibition of PI3K signaling pathways that are significant in governing synaptic plasticity, which impairment hallmarks the early stage of AD [77–79]. The modulation of the serotonin/G-protein coupled receptor/PI3K/Akt signaling pathway has been debated as possible for AD prevention and therapy through mitigating abnormal synaptic activities induced by A β and tau proteins [80–82]. Additionally, the PI3K/Akt signaling pathway is intimately related to A β induced apoptosis. The activation of the PI3K-Akt signaling pathway can prevent neuronal loss by suppressing pro-apoptosis protein (i.e., CASP3 and p53) and by activating anti-apoptotic protein (i.e., BCL2) [83,84]. Apart from these, the significantly enriched GO terms in biological process (BP) include response to oxygen levels, neuron apoptotic process, and regulation of inflammatory response. Together, a reasonable deduction is that abnormal accumulation of A β and tau accompanied by oxidative stress mutually modulate the p53/PI3K/Akt signaling pathway and further induce neuronal apoptosis and impair synaptic plasticity, wherein the mechanism of active components in EZW against AD underlying the whole process.

To further achieve the core targets with therapeutic potentials in clinical practice, we performed an in-depth validation with approaches of bioinformatics tools, molecular docking, and molecular dynamics (MD) simulations. We identified 41 out of 140 targets that correlated with A β and tau. Among these, we found 25 targets differentially expressed in the hippocampus, entorhinal cortex, frontal cortex, or temporal cortex between control and AD patient samples from GEO datasets. Then, we conducted the molecular docking and binding pocket prediction to assess the binding affinity and pocket druggability. We found 18 docking pairs exhibiting favorable binding affinities and binding sites. As previously demonstrated that the hippocampus served a pivotal role in the unveiled

mechanism, we selected targets differentially expressed in the hippocampus for further presentation and evaluation. Accordingly, we obtained five protein-ligand complexes including AR-acacetin, AR-pratensein, CASP8-acacetin, POLB- β -sitosterol, and PREP-3-O-acetyldammareniol-II. Notably, POLB and PREP are differentially expressed across four brain regions, while AR is the seed node of MCODE cluster 1. These indicate the predominant roles of AR, POLB, and PREP in the mechanism of EZW against AD. Afterward, we performed molecular docking with positive ligand controls to validate the biological functions of the binding pockets and the docking parameters. Through literature research, we identified the role of ligand-binding pockets for each target protein and selected the ligand control accordingly. The binding poses between AR, CASP8, POLB, and PREP and their respective ligand controls have been experimentally validated with crystal structure models [85–88].

The binding pocket of AR is highlighted by the interaction with ARG752, a binding site for natural androgen dihydrotestosterone (DHT) [85]. The observations of sex differences and hormonal alterations in the incidence of AD have long been noted, as women exhibited a two-fold risk of developing late-onset AD than men [89]. Age-related serum androgen depletion (i.e. testosterone) correlated with the pathological events of AD in elderly males. On the contrary, an increased serum testosterone level displayed neuroprotective abilities and ameliorated cognitive and behavioral processes [90]. In the AD mice model, endogenous testosterone can reduce A β deposit by downregulating the expression level of BACE1 [91]. AR is distributed in multiple brain regions, especially the hippocampus that involved in learning and memory abilities [92]. In the AD rat model, testosterone can mitigate oxidative stress and facilitate the dendritic spine density in the hippocampus CA1 region in an AR-dependent manner [93]. On the cellular level, androgens can elongate the neurite outgrowth and ameliorate oxidative stress-induced cell death through an AR-dependent mechanism [94,95]. Additionally, the depletion of AR eliminated the protective effects of androgens against tau pathology through the PI3K/Akt/GSK3 β signaling pathway in the PC12 cell model [96]. Together, these studies underscore the crucial roles of androgens and AR in combating AD, and acacetin and pratensein could potentially function as alternatives to androgens. Caspase-8 (CASP8) is a pivotal initiator of several cell death pathways induced by death receptor interactions. Upon activation, caspase-8 is recruited, followed by coordinated dimerization and cleavage, and subsequently initiates apoptosis through activating effector caspases or interacting with BCL2 family members [97,98]. In AD pathology, caspase-8 can be activated by A β , leading to neuronal death [99]. Likewise, inhibition of caspase-8 by small molecules conferred neuroprotection in rats injected with A β and alleviated cognitive impairment [100]. Additionally, activated caspase-8 was reported to cleave APP at position 664 in the presence of A β and induce synapse loss [101]. Caspase inhibition has been proposed as a potentially novel therapeutic option [102,103]. In our study, acacetin binds to a pocket close to SER375, ASP384, and LEU385 residues. Notably, residues 374–375 in caspase-8 serve as a cleavage site for caspase-6, while residues 384–385 represent an auto-cleavage site, and both are significant in programmed cell death [63,104]. Caspase-6 can be directly regulated by p53, and its knockout in the 5xFAD AD model improved memory deficits [105]. Moreover, intense fluctuations of residues 370–385 are observed in the MD simulation study, which might explain the inhibitory role of acacetin in caspase-8. Despite these findings, the acacetin-binding pocket of caspase-8 is not a primary active site, which might require further attention [86]. POLB plays a significant role in the base-excision repair (BER) pathway for DNA damage repair, which maintains genomic stability [106]. The deficiency of POLB resulting from aging can exacerbate AD symptoms by inducing oxidative stress and impairing synaptic plasticity, and interventions to sustain the POLB level can reduce the risks of AD [107]. This is consistent with the findings that oxidative stress induced DNA damage would lead to cognitive impairment in AD patients, which manifests the neuroprotective role of POLB [108]. However, inhibition of POLB through small molecules can reduce neuron death against A β neurotoxicity *in vitro* and *in vivo* studies [109,110]. This dilemma might be reconciled by the discovery that POLB is implicated with the A β induced cell cycle reentry, and ensuing neuronal apoptosis [111,112]. Through molecular docking investigation, we found β -sitosterol can bind to the active site of POLB competing with deoxyribonucleotide triphosphate (dNTP) [87]. β -sitosterol interacts with residues ASP190, ASP192, ASP276, LYS280, and ARG283, which are crucial in the activity and fidelity of POLB [113]. The MD simulation of the POLB- β -sitosterol complex manifests the conformational alteration of the protein. The ROG and SASA values decrease across the simulation period, which facilitates complex stability and might prevent additional ligand bindings. Moreover, the functions of POLB are intimately associated with the p53/PI3K/Akt signaling pathway, as p53 can stabilize the interaction between POLB and DNA backbone, while PI3K/Akt induces the expression of APE1, a significant enzyme in the BER pathway [114,115]. PREP is a peptidase able for short peptides hydrolyzation highly expressed in the brain region [116]. Accordingly, it can modulate the neuropeptide level in the brain, yet its physiological substrate remains unconcluded [117]. Neuropeptides are crucial in extensive brain functions including cognition, memory, and learning [118]. PREP also functions through protein-protein interaction, as its colocalization with A β plaque and tau protein has been observed in AD patients [119]. Inhibition of PREP results in a significant decrease in A β and tau aggregation and alleviation of oxidative stress, while the mechanism is still in debate [120]. PREP comprises two distinctive domains: a protease catalytic domain (residues 1–71 and 436–710) and a β -propeller domain (residues 72–435). The propeller domain mainly functions as a substrate gate (~4 Å in bottom entrance) that merely permits the access of short peptides to the catalytic site [121]. Our results suggest that 3-O-acetyldammareniol-II interacts with the β -propeller domain of PREP similar to a synthetic unnatural dipeptide inhibitor [88]. This indicates 3-O-acetyldammareniol-II potentially inhibits PREP by obstructing short peptide entrance. The stabilities of five docking pairs were further evaluated by the MD simulations approach. RMSD values of the complexes are less than 1 nm across the simulation periods, indicating that the systems stabilize under near-physiological conditions. The MM/PBSA strategy was employed to re-demonstrate the binding pose and affinity between ligands and proteins. The calculated mean value of binding free energies (BFEs) ranges from -11.66 to -92.28 kJ/mol, manifesting strong affinities except for the AR-pratensein complex. The compromised stability of AR-partensein can partially be explained by the free energy landscape (FEL) plot and interaction entropy terms, that a continuous alteration of ligand-binding poses in the protein pocket might exist. Decompositions of MM/PBSA energies per residue display the significant interactions between the ligands and the proteins. The interaction analyses of complex conformations in the minimum energy basins of FELs re-confirm the pivotal roles of these residues in binding modes. Further examination of hydrogen

bonding patterns suggests that AR-acacetin and CASP8-acacetin form relatively stable hydrogen bonds. The interaction analyses manifest the predominant roles of Pi-Alkyl and Alkyl interactions in the POLB- β -sitosterol complex, and van der Waals interaction in the PREP-3-O-acetyldammarenediol-II complex. Together, acacetin, β -sitosterol, and 3-O-acetyldammarenediol-II exhibit potential as small molecular drugs in AD therapy by targeting AR, CASP8, POLB, and PREP.

Despite the encouraging discoveries in the mechanisms of EZW against AD, there are still certain limitations. Firstly, the present study is mostly established on existing databases and thus might yield inadequate inference if the databases were not fully comprehensive and reviewed. Additionally, the combined roles of the active components in activating or inhibiting the AD-relevant pathways remain unknown. Moreover, although we take a step forward in the systemic demonstration of EZW efficacy, the determined active components and targets can't represent the holistic effects across the body. Since our study mainly relies on *in-silica* approaches, future *in vivo* and *in vitro* experimental validations are needed to reinforce our findings.

5. Conclusion

To summarize, our study, for the first time, explored the active components and the mechanism of EZW in treating AD through a multi-disciplinary strategy. Based on a network pharmacology approach, acacetin, β -sitosterol, pratensein, and 3-O-acetyldammarenediol-II were identified as the active components of EZW with BBB permeability and potentially exerted therapeutic effects on AD through regulating p53/PIK3/Akt signaling pathways that related to A β and tau pathology, oxidative stress, synaptic plasticity, and neuronal apoptosis. Moreover, we employed a combination approach of bioinformatics analysis, molecular docking, and molecular dynamics simulation to validate the previous predictions, and found acacetin, β -sitosterol, and 3-O-acetyldammarenediol-II could stably bind to AR, CASP8, POLB, and PREP, which were druggable targets enriched in the hippocampus. Overall, our study demonstrated a multi-component and multi-target basis to combat AD and provided a promising reference for subsequent research regarding drug discovery and clinical applications.

Funding statement

This work was supported by the grant (ZR2021QH238) of Shandong Province Natural Science Foundation, the grant (202313051720) of Shandong Province Medical and Health Technology project, and the grant (2022KJ255) of the College Youth Innovation Team of Shandong Province.

Ethics statement

Not applicable.

Data availability statement

Data were included in article/supplementary material/referenced in article. The raw and processed sequencing datasets derived from the Alzdata website are available at the NCBI GEO under the following accession numbers: (1) Frontal Cortex: GSE12685, GSE36980, GSE48350, GSE5281, GSE53890, GSE66333, GSE15222; (2) Temporal Cortex: GSE29652, GSE36980, GSE37263, GSE5281; (3) Hippocampus: GSE28146, GSE29378, GSE36980, GSE48350, GSE5281; (4) Entorhinal Cortex: GSE26927, GSE26972, GSE48350, GSE5281.

CRedit authorship contribution statement

Meng Yu: Writing – review & editing, Writing – original draft, Visualization, Software, Resources, Formal analysis, Data curation, Conceptualization. **Zhongqi Shen:** Writing – review & editing, Visualization, Software, Resources, Methodology, Formal analysis, Data curation, Conceptualization. **Shaozhi Zhang:** Writing – review & editing, Investigation, Funding acquisition, Conceptualization. **Yang Zhang:** Writing – review & editing, Investigation. **Hongwei Zhao:** Writing – review & editing, Validation, Supervision, Project administration. **Longfei Zhang:** Writing – review & editing, Validation, Supervision, Project administration, Methodology, Funding acquisition.

Declaration of competing interest

None Declared.

Acknowledgement

We thank for the assistance of Shandong University of Traditional Chinese Medicine.

Appendix A. Supplementary data

Supplementary data to this article can be found online at <https://doi.org/10.1016/j.heliyon.2024.e33761>.

References

- [1] G.B.D.D.F. Collaborators, Estimation of the global prevalence of dementia in 2019 and forecasted prevalence in 2050: an analysis for the Global Burden of Disease Study 2019, *Lancet Public Health* 7 (2) (2022) e105–e125.
- [2] B. Dubois, N. Villain, G.B. Frisoni, G.D. Rabinovici, M. Sabbagh, S. Cappa, A. Bejanin, S. Bombois, S. Epelbaum, M. Teichmann, et al., Clinical diagnosis of Alzheimer's disease: recommendations of the International working group, *Lancet Neurol.* 20 (6) (2021) 484–496.
- [3] S. Srivastava, R. Ahmad, S.K. Khare, Alzheimer's disease and its treatment by different approaches: a review, *Eur. J. Med. Chem.* 216 (2021) 113320.
- [4] C.A. Lane, J. Hardy, J.M. Schott, Alzheimer's disease, *Eur. J. Neurol.* 25 (1) (2018) 59–70.
- [5] E. Tonnes, E. Trushina, Oxidative stress, synaptic dysfunction, and Alzheimer's disease, *J Alzheimers Dis* 57 (4) (2017) 1105–1121.
- [6] J.W. Kinney, S.M. Bemiller, A.S. Murtishaw, A.M. Leisgang, A.M. Salazar, B.T. Lamb, Inflammation as a central mechanism in Alzheimer's disease, *Alzheimers Dement (N Y)* 4 (2018) 575–590.
- [7] C. Iadecola, M. Duering, V. Hachinski, A. Joutel, S.T. Pendlebury, J.A. Schneider, M. Dichgans, Vascular cognitive impairment and dementia: JACC Scientific Expert Panel, *J. Am. Coll. Cardiol.* 73 (25) (2019) 3326–3344.
- [8] J. Cummings, N. Fox, Defining disease modifying therapy for Alzheimer's disease, *J Prev Alzheimers Dis* 4 (2) (2017) 109–115.
- [9] P. Scheltens, B. De Strooper, M. Kivipelto, H. Holstege, G. Chetelat, C.E. Teunissen, J. Cummings, van der Flier WM: Alzheimer's disease, *Lancet* 397 (10284) (2021) 1577–1590.
- [10] J. Cummings, G. Lee, P. Nahed, M. Kamar, K. Zhong, J. Fonseca, K. Taghva, Alzheimer's disease drug development pipeline: 2022, *Alzheimers Dement (N Y)* 8 (1) (2022) e12295.
- [11] F. Mangialasche, A. Solomon, B. Winblad, P. Mecocci, M. Kivipelto, Alzheimer's disease: clinical trials and drug development, *Lancet Neurol.* 9 (7) (2010) 702–716.
- [12] M. Safieh, A.D. Korczyn, D.M. Michaelson, ApoE4: an emerging therapeutic target for Alzheimer's disease, *BMC Med.* 17 (1) (2019) 64.
- [13] Y. Ju, K.Y. Tam, Pathological mechanisms and therapeutic strategies for Alzheimer's disease, *Neural Regen Res* 17 (3) (2022) 543–549.
- [14] C. Nogales, Z.M. Mamdouh, M. List, C. Kiel, A.I. Casas, H. Schmidt, Network pharmacology: curing causal mechanisms instead of treating symptoms, *Trends Pharmacol. Sci.* 43 (2) (2022) 136–150.
- [15] A.P. Lu, H.W. Jia, C. Xiao, Q.P. Lu, Theory of traditional Chinese medicine and therapeutic method of diseases, *World J. Gastroenterol.* 10 (13) (2004) 1854–1856.
- [16] X. Zhou, S.W. Seto, D. Chang, H. Kiat, V. Razmovski-Naumovski, K. Chan, A. Bensoussan, Synergistic effects of Chinese herbal medicine: a comprehensive review of methodology and current research, *Front. Pharmacol.* 7 (2016) 201.
- [17] L.C. Matos, J.P. Machado, F.J. Monteiro, H.J. Greten, Understanding traditional Chinese medicine therapeutics: an overview of the Basics and clinical applications, *Healthcare (Basel)* 9 (3) (2021).
- [18] S. Li, Z. Wu, W. Le, Traditional Chinese medicine for dementia, *Alzheimers Dement* 17 (6) (2021) 1066–1071.
- [19] Y.S. Ho, K.F. So, R.C. Chang, Drug discovery from Chinese medicine against neurodegeneration in Alzheimer's and vascular dementia, *Chin. Med.* 6 (2011) 15.
- [20] Y. Zhai, J. Xu, L. Feng, Q. Liu, W. Yao, H. Li, Y. Cao, F. Cheng, B. Bao, L. Zhang, Broad range metabolomics coupled with network analysis for explaining possible mechanisms of Er-Zhi-Wan in treating liver-kidney Yin deficiency syndrome of Traditional Chinese medicine, *J. Ethnopharmacol.* 234 (2019) 57–66.
- [21] L. Feng, Y.Y. Zhai, J. Xu, W.F. Yao, Y.D. Cao, F.F. Cheng, B.H. Bao, L. Zhang, A review on traditional uses, phytochemistry and pharmacology of *Eclipta prostrata* (L.) L, *J. Ethnopharmacol.* 245 (2019) 112109.
- [22] Y.J. Kim, S.Y. Park, Y.J. Koh, J.H. Lee, Anti-neuroinflammatory effects and mechanism of action of *Fructus ligustri lucidi* Extract in BV2 Microglia, *Plants* 10 (4) (2021).
- [23] Y. Xie, B. Yan, M. Hou, M. Zhou, C. Liu, M. Sun, K. He, C. Fang, Y. Chen, L. Huang, Erzhi pills ameliorate cognitive dysfunction and alter proteomic hippocampus profiles induced by d-galactose and Abeta(1-)(40) injection in ovarietomized Alzheimer's disease model rats, *Pharm. Biol.* 59 (1) (2021) 1402–1414.
- [24] Y.N. Dai, Y. Wang, Z.J. Zhang, W.X. Tan, X.Y. Wang, X.M. Gao, Erzhi Pill regulates lipid metabolism and prevents atherosclerosis in ovarietomized ApoE-deficient mice, *J. Am. Coll. Cardiol.* 72 (16) (2018) C80. C80.
- [25] M. Kibble, N. Saarinen, J. Tang, K. Wennerberg, S. Makela, T. Aittokallio, Network pharmacology applications to map the unexplored target space and therapeutic potential of natural products, *Nat. Prod. Rep.* 32 (8) (2015) 1249–1266.
- [26] T. Barrett, S.E. Wilhite, P. Ledoux, C. Evangelista, L.F. Kim, M. Tomashevsky, K.A. Marshall, K.H. Phillippy, P.M. Sherman, M. Holko, et al., NCBI GEO: archive for functional genomics data sets—update, *Nucleic Acids Res.* 41 (Database issue) (2013) D991–D995.
- [27] N. Schaduengrat, S. Lampa, S. Simeon, M.P. Gleeson, O. Spjuth, C. Nantasenamat, Towards reproducible computational drug discovery, *J Cheminform* 12 (1) (2020) 9.
- [28] F.E. Agamah, G.K. Mazandu, R. Hassan, C.D. Bope, N.E. Thomford, A. Ghansah, E.R. Chimusa, Computational/in silico methods in drug target and lead prediction, *Brief Bioinform* 21 (5) (2020) 1663–1675.
- [29] Y. Zhang, M. Luo, P. Wu, S. Wu, T.Y. Lee, C. Bai, Application of computational biology and Artificial Intelligence in drug Design, *Int. J. Mol. Sci.* 23 (21) (2022).
- [30] J. Ru, P. Li, J. Wang, W. Zhou, B. Li, C. Huang, P. Li, Z. Guo, W. Tao, Y. Yang, et al., TCMSP: a database of systems pharmacology for drug discovery from herbal medicines, *J Cheminform* 6 (2014) 13.
- [31] X. Xu, W. Zhang, C. Huang, Y. Li, H. Yu, Y. Wang, J. Duan, Y. Ling, A novel chemometric method for the prediction of human oral bioavailability, *Int. J. Mol. Sci.* 13 (6) (2012) 6964–6982.
- [32] S. Tian, J. Wang, Y. Li, D. Li, L. Xu, T. Hou, The application of in silico drug-likeness predictions in pharmaceutical research, *Adv. Drug Deliv. Rev.* 86 (2015) 2–10.
- [33] P. Artursson, K. Palm, K. Luthman, Caco-2 monolayers in experimental and theoretical predictions of drug transport, *Adv. Drug Deliv. Rev.* 46 (1–3) (2001) 27–43.
- [34] C.A. Lipinski, F. Lombardo, B.W. Dominy, P.J. Feeney, Experimental and computational approaches to estimate solubility and permeability in drug discovery and development settings, *Adv. Drug Deliv. Rev.* 46 (1–3) (2001) 3–26.
- [35] A. Daina, O. Michielin, V. Zoete, SwissADME: a free web tool to evaluate pharmacokinetics, drug-likeness and medicinal chemistry friendliness of small molecules, *Sci. Rep.* 7 (2017) 42717.
- [36] D. Gfeller, A. Grosdidier, M. Wirth, A. Daina, O. Michielin, V. Zoete, SwissTargetPrediction: a web server for target prediction of bioactive small molecules, *Nucleic Acids Res.* 42 (Web Server issue) (2014) W32–W38.
- [37] X. Liu, S. Ouyang, B. Yu, Y. Liu, K. Huang, J. Gong, S. Zheng, Z. Li, H. Li, H. Jiang, PharmMapper server: a web server for potential drug target identification using pharmacophore mapping approach, *Nucleic Acids Res.* 38 (Web Server issue) (2010) W609–W614.
- [38] Q. Lv, G. Chen, H. He, Z. Yang, L. Zhao, K. Zhang, C.Y. Chen, TCMBank-the largest TCM database provides deep learning-based Chinese-Western medicine exclusion prediction, *Signal Transduct Target Ther* 8 (1) (2023) 127.
- [39] M. Safran, I. Dalah, J. Alexander, N. Rosen, T. Iny Stein, M. Shmoish, N. Nativ, I. Bahir, T. Doniger, H. Krug, et al., GeneCards Version 3: the human gene integrator, *Database* 2010 (2010) baq020.
- [40] G.R. Brown, V. Hem, K.S. Katz, M. Ovetsky, C. Wallin, O. Ermolaeva, I. Tolstoy, T. Tatusova, K.D. Pruitt, D.R. Maglott, et al., Gene: a gene-centered information resource at NCBI, *Nucleic Acids Res.* 43 (Database issue) (2015) D36–D42.
- [41] J.S. Amberger, C.A. Bocchini, F. Schiettecatte, A.F. Scott, A. Hamosh, OMIM.org: online Mendelian Inheritance in Man (OMIM(R)), an online catalog of human genes and genetic disorders, *Nucleic Acids Res.* 43 (Database issue) (2015) D789–D798.
- [42] P. Shannon, A. Markiel, O. Ozier, N.S. Baliga, J.T. Wang, D. Ramage, N. Amin, B. Schwikowski, T. Ideker, Cytoscape: a software environment for integrated models of biomolecular interaction networks, *Genome Res.* 13 (11) (2003) 2498–2504.

- [43] C. von Mering, M. Huynen, D. Jaeggi, S. Schmidt, P. Bork, B. Snel, STRING: a database of predicted functional associations between proteins, *Nucleic Acids Res.* 31 (1) (2003) 258–261.
- [44] G.D. Bader, C.W. Hogue, An automated method for finding molecular complexes in large protein interaction networks, *BMC Bioinf.* 4 (2003) 2.
- [45] T. Wu, E. Hu, S. Xu, M. Chen, P. Guo, Z. Dai, T. Feng, L. Zhou, W. Tang, L. Zhan, et al., clusterProfiler 4.0: a universal enrichment tool for interpreting omics data, *Innovation* 2 (3) (2021) 100141.
- [46] M. Xu, D.F. Zhang, R. Luo, Y. Wu, H. Zhou, L.L. Kong, R. Bi, Y.G. Yao, A systematic integrated analysis of brain expression profiles reveals YAP1 and other prioritized hub genes as important upstream regulators in Alzheimer's disease, *Alzheimers Dement* 14 (2) (2018) 215–229.
- [47] X.Y. Meng, H.X. Zhang, M. Mezei, M. Cui, Molecular docking: a powerful approach for structure-based drug discovery, *Curr. Comput. Aided Drug Des.* 7 (2) (2011) 146–157.
- [48] D. Seeliger, B.L. de Groot, Ligand docking and binding site analysis with PyMOL and Autodock/Vina, *J. Comput. Aided Mol. Des.* 24 (5) (2010) 417–422.
- [49] J. Westbrook, Z. Feng, S. Jain, T.N. Bhat, N. Thanki, V. Ravichandran, G.L. Gilliland, W. Bluhm, H. Weissig, D.S. Greer, et al., The protein Data Bank: unifying the archive, *Nucleic Acids Res.* 30 (1) (2002) 245–248.
- [50] A. Waterhouse, M. Bertoni, S. Bienert, G. Studer, G. Tauriello, R. Gumienny, F.T. Heer, T.A.P. de Beer, C. Rempfer, L. Bordoli, et al., SWISS-MODEL: homology modelling of protein structures and complexes, *Nucleic Acids Res.* 46 (W1) (2018) W296–W303.
- [51] X. Li, S. Wei, S. Niu, X. Ma, H. Li, M. Jing, Y. Zhao, Network pharmacology prediction and molecular docking-based strategy to explore the potential mechanism of Huanglian Jiedu Decoction against sepsis, *Comput. Biol. Med.* 144 (2022) 105389.
- [52] A. Volkamer, D. Kuhn, T. Grombacher, F. Rippmann, M. Rarey, Combining global and local measures for structure-based druggability predictions, *J. Chem. Inf. Model.* 52 (2) (2012) 360–372.
- [53] D. Van Der Spoel, E. Lindahl, B. Hess, G. Groenhof, A.E. Mark, H.J. Berendsen, GROMACS: fast, flexible, and free, *J. Comput. Chem.* 26 (16) (2005) 1701–1718.
- [54] L.L. Duan, X. Liu, J.Z.H. Zhang, Interaction entropy: a New Paradigm for highly Efficient and reliable computation of protein-ligand binding free energy, *J. Am. Chem. Soc.* 138 (17) (2016) 5722–5728.
- [55] J. Petit, N. Meurice, C. Kaiser, G. Maggiora, Softening the rule of five—where to draw the line? *Bioorg. Med. Chem.* 20 (18) (2012) 5343–5351.
- [56] V. Ivanović, M. Ranić, B. Arsić, A. Pavlović, Lipinski's rule of five, famous extensions and famous exceptions, *Popular Scientific Article* 3 (1) (2020) 171–177.
- [57] M. Jorfi, A. Maaser-Hecker, R.E. Tanzi, The neuroimmune axis of Alzheimer's disease, *Genome Med.* 15 (1) (2023) 6.
- [58] Z.H. Liu, Y.J. Wang, X.L. Bu, Alzheimer's disease: targeting the peripheral circulation, *Mol. Neurodegener.* 18 (1) (2023) 3.
- [59] J.L. Cummings, A.M.L. Osse, J.W. Kinney, Alzheimer's disease: novel targets and investigational drugs for disease Modification, *Drugs* 83 (15) (2023) 1387–1408.
- [60] T.S. Salameh, E.M. Rhea, K. Talbot, W.A. Banks, Brain uptake pharmacokinetics of incretin receptor agonists showing promise as Alzheimer's and Parkinson's disease therapeutics, *Biochem. Pharmacol.* 180 (2020) 114187.
- [61] Z.J. Wang, X.R. Li, S.F. Chai, W.R. Li, S. Li, M. Hou, J.L. Li, Y.C. Ye, H.Y. Cai, C. Holscher, et al., Semaglutide ameliorates cognition and glucose metabolism dysfunction in the 3xTg mouse model of Alzheimer's disease via the GLP-1R/SIRT1/GLUT4 pathway, *Neuropharmacology* 240 (2023) 109716.
- [62] H. Yang, W. Zhang, C. Huang, W. Zhou, Y. Yao, Z. Wang, Y. Li, W. Xiao, Y. Wang, A novel systems pharmacology model for herbal medicine injection: a case using Reduning injection, *BMC Complement Altern Med* 14 (2014) 430.
- [63] X. Li, F. Li, X. Zhang, H. Zhang, Q. Zhao, M. Li, X. Wu, L. Wang, J. Liu, X. Wu, et al., Caspase-8 auto-cleavage regulates programmed cell death and collaborates with RIPK3/MLKL to prevent lymphopenia, *Cell Death Differ.* 29 (8) (2022) 1500–1512.
- [64] L. Polgar, A. Patthy, Cleavage of the Lys196-Ser197 bond of prolyl oligopeptidase: enhanced catalytic activity for one of the two active enzyme forms, *Biochemistry* 31 (44) (1992) 10769–10773.
- [65] O.K. Mankoo, A. Kaur, D. Goyal, B. Goyal, Unravelling the destabilization potential of ellagic acid on alpha-synuclein fibrils using molecular dynamics simulations, *Phys. Chem. Chem. Phys.* 25 (11) (2023) 8128–8143.
- [66] S. Genheden, U. Ryde, The MM/PBSA and MM/GBSA methods to estimate ligand-binding affinities, *Expert Opin Drug Dis* 10 (5) (2015) 449–461.
- [67] M.S. Valdes-Tresanco, M.E. Valdes-Tresanco, P.A. Valiente, E. Moreno, gmx_MMPBSA: a New tool to perform End-state free energy calculations with GROMACS, *J. Chem. Theor. Comput.* 17 (10) (2021) 6281–6291.
- [68] X. Wang, H. Perumalsamy, H.W. Kwon, Y.E. Na, Y.J. Ahn, Effects and possible mechanisms of action of acacetin on the behavior and eye morphology of *Drosophila* models of Alzheimer's disease, *Sci. Rep.* 5 (2015) 16127.
- [69] X. Zhang, W. Song, The role of APP and BACE1 trafficking in APP processing and amyloid-beta generation, *Alzheimer's Res. Ther.* 5 (5) (2013) 46.
- [70] S. Lee, K. Youn, M. Jun, Major compounds of red ginseng oil attenuate Abeta(25-35)-induced neuronal apoptosis and inflammation by modulating MAPK/NF-kappaB pathway, *Food Funct.* 9 (8) (2018) 4122–4134.
- [71] C. Cheignon, M. Tomas, D. Bonnefont-Rousselot, P. Faller, C. Hureau, F. Collin, Oxidative stress and the amyloid beta peptide in Alzheimer's disease, *Redox Biol.* 14 (2018) 450–464.
- [72] C. Liang, S. Tan, Q. Huang, J. Lin, Z. Lu, X. Lin, Pratensein ameliorates beta-amyloid-induced cognitive impairment in rats via reducing oxidative damage and restoring synapse and BDNF levels, *Neurosci. Lett.* 592 (2015) 48–53.
- [73] L. Zou, Z. Wang, L. Shen, G.B. Bao, T. Wang, J.H. Kang, G. Pei, Receptor tyrosine kinases positively regulate BACE activity and Amyloid-beta production through enhancing BACE internalization, *Cell Res.* 17 (5) (2007) 389–401.
- [74] G. Dhawan, C.K. Combs, Inhibition of Src kinase activity attenuates amyloid associated microgliosis in a murine model of Alzheimer's disease, *J. Neuroinflammation* 9 (2012) 117.
- [75] S.L. Ma, N.L. Tang, Y.P. Zhang, L.D. Ji, C.W. Tam, V.W. Lui, H.F. Chiu, L.C. Lam, Association of prostaglandin-endoperoxide synthase 2 (PTGS2) polymorphisms and Alzheimer's disease in Chinese, *Neurobiol. Aging* 29 (6) (2008) 856–860.
- [76] D. Singh, S.K. Srivastava, T.K. Chaudhuri, G. Upadhyay, Multifaceted role of matrix metalloproteinases (MMPs), *Front. Mol. Biosci.* 2 (2015) 19.
- [77] P.K. Jayaswamy, M. Vijaykrishnaraj, P. Patil, L.M. Alexander, A. Kellarai, P. Shetty, Implicative role of epidermal growth factor receptor and its associated signaling partners in the pathogenesis of Alzheimer's disease, *Ageing Res. Rev.* 83 (2023) 101791.
- [78] L. Wang, H.C. Chiang, W. Wu, B. Liang, Z. Xie, X. Yao, W. Ma, S. Du, Y. Zhong, Epidermal growth factor receptor is a preferred target for treating amyloid-beta-induced memory loss, *Proc Natl Acad Sci U S A* 109 (41) (2012) 16743–16748.
- [79] R. Akhter, P. Sanphui, S.C. Biswas, The essential role of p53-up-regulated modulator of apoptosis (Puma) and its regulation by FoxO3a transcription factor in beta-amyloid-induced neuron death, *J. Biol. Chem.* 289 (15) (2014) 10812–10822.
- [80] C.L. Busceti, P. Di Pietro, B. Rizzio, A. Traficante, F. Biagioni, R. Nistico, F. Fornai, G. Battaglia, F. Nicoletti, V. Bruno, 5-HT_{2C} serotonin receptor blockade prevents tau protein hyperphosphorylation and corrects the defect in hippocampal synaptic plasticity caused by a combination of environmental stressors in mice, *Pharmacol. Res.* 99 (2015) 258–268.
- [81] S. Shahidi, N. Hashemi-Firouzi, S.S. Asl, A. Komaki, Serotonin type 6 receptor antagonist attenuates the impairment of long-term potentiation and memory induced by Abeta, *Behav. Brain Res.* 364 (2019) 205–212.
- [82] N. Nakano, S. Matsuda, M. Ichimura, A. Minami, M. Ogino, T. Murai, Y. Kitagishi, PI3K/AKT signaling mediated by G protein-coupled receptors is involved in neurodegenerative Parkinson's disease, *Int. J. Mol. Med.* 39 (2) (2017) 253–260.
- [83] H.Z. Long, Y. Cheng, Z.W. Zhou, H.Y. Luo, D.D. Wen, L.C. Gao, PI3K/AKT signal pathway: a target of natural products in the prevention and treatment of Alzheimer's disease and Parkinson's disease, *Front. Pharmacol.* 12 (2021) 648636.
- [84] S. Kumari, R. Dhapola, D.H. Reddy, Apoptosis in Alzheimer's disease: insight into the signaling pathways and therapeutic avenues, *Apoptosis* 28 (7–8) (2023) 943–957.
- [85] K. Pereira de Jesus-Tran, P.L. Cote, L. Cantin, J. Blanchet, F. Labrie, R. Breton, Comparison of crystal structures of human androgen receptor ligand-binding domain complexed with various agonists reveals molecular determinants responsible for binding affinity, *Protein Sci.* 15 (5) (2006) 987–999.

- [86] Z. Wang, W. Watt, N.A. Brooks, M.S. Harris, J. Urban, D. Boatman, M. McMillan, M. Kahn, R.L. Heinrikson, B.C. Finzel, et al., Kinetic and structural characterization of caspase-3 and caspase-8 inhibition by a novel class of irreversible inhibitors, *Biochim. Biophys. Acta* 1804 (9) (2010) 1817–1831.
- [87] H. Pelletier, M.R. Saway, W. Wolfle, S.H. Wilson, J. Kraut, A structural basis for metal ion mutagenicity and nucleotide selectivity in human DNA polymerase beta, *Biochemistry* 35 (39) (1996) 12762–12777.
- [88] D.T. Racys, D. Rea, V. Fulop, M. Wills, Inhibition of prolyl oligopeptidase with a synthetic unnatural dipeptide, *Bioorg. Med. Chem.* 18 (13) (2010) 4775–4782.
- [89] J.L. Podcasy, C.N. Epperson, Considering sex and gender in Alzheimer disease and other dementias, *Dialogues Clin. Neurosci.* 18 (4) (2016) 437–446.
- [90] V.E. Bianchi, Impact of testosterone on Alzheimer's disease, *World J Mens Health* 40 (2) (2022) 243–256.
- [91] C. McAllister, J. Long, A. Bowers, A. Walker, P. Cao, S. Honda, N. Harada, M. Staufenbiel, Y. Shen, R. Li, Genetic targeting aromatase in male amyloid precursor protein transgenic mice down-regulates beta-secretase (BACE1) and prevents Alzheimer-like pathology and cognitive impairment, *J. Neurosci.* 30 (21) (2010) 7326–7334.
- [92] J.E. Kerr, R.J. Allore, S.G. Beck, R.J. Handa, Distribution and hormonal regulation of androgen receptor (AR) and AR messenger ribonucleic acid in the rat hippocampus, *Endocrinology* 136 (8) (1995) 3213–3221.
- [93] X.S. Yan, Z.J. Yang, J.X. Jia, W. Song, X. Fang, Z.P. Cai, D.S. Huo, H. Wang, Protective mechanism of testosterone on cognitive impairment in a rat model of Alzheimer's disease, *Neural Regen Res* 14 (4) (2019) 649–657.
- [94] T.U. Marron, V. Guerini, P. Rusmini, D. Sau, T.A. Brevini, L. Martini, A. Poletti, Androgen-induced neurite outgrowth is mediated by neurtin in motor neurones, *J. Neurochem.* 92 (1) (2005) 10–20.
- [95] E. Ahlbom, G.S. Prins, S. Ceccatelli, Testosterone protects cerebellar granule cells from oxidative stress-induced cell death through a receptor mediated mechanism, *Brain Res.* 892 (2) (2001) 255–262.
- [96] M. Yao, E.R. Rosario, J.C. Soper, C.J. Pike, Androgens regulate tau phosphorylation through Phosphatidylinositol 3-kinase-protein kinase B-Glycogen synthase kinase 3beta signaling, *Neuroscience* (2022).
- [97] C. Scaffidi, S. Fulda, A. Srinivasan, C. Friesen, F. Li, K.J. Tomaselli, K.M. Debatin, P.H. Kramer, M.E. Peter, Two CD95 (APO-1/Fas) signaling pathways, *EMBO J.* 17 (6) (1998) 1675–1687.
- [98] A. Oberst, C. Pop, A.G. Tremblay, V. Blais, J.B. Denault, G.S. Salvesen, D.R. Green, Inducible dimerization and inducible cleavage reveal a requirement for both processes in caspase-8 activation, *J. Biol. Chem.* 285 (22) (2010) 16632–16642.
- [99] W. Wei, D.D. Norton, X. Wang, J.W. Kusiak, Abeta 17-42 in Alzheimer's disease activates JNK and caspase-8 leading to neuronal apoptosis, *Brain* 125 (Pt 9) (2002) 2036–2043.
- [100] J.J. Miguel-Hidalgo, I.A. Paul, V. Wanzo, P.K. Banerjee, Memantine prevents cognitive impairment and reduces Bcl-2 and caspase 8 immunoreactivity in rats injected with amyloid beta1-40, *Eur. J. Pharmacol.* 692 (1–3) (2012) 38–45.
- [101] G. Park, H.S. Nhan, S.H. Tyan, Y. Kawakatsu, C. Zhang, M. Navarro, E.H. Koo, Caspase activation and caspase-mediated cleavage of APP is associated with amyloid beta-protein-induced synapse loss in Alzheimer's disease, *Cell Rep.* 31 (13) (2020) 107839.
- [102] C.M. Troy, Y.Y. Jean, Caspases: therapeutic targets in neurologic disease, *Neurotherapeutics* 12 (1) (2015) 42–48.
- [103] T.T. Rohm, The role of caspases in Alzheimer's disease; potential novel therapeutic opportunities, *Apoptosis* 15 (11) (2010) 1403–1409.
- [104] B.J. van Raam, D.E. Ehrnhoefer, M.R. Hayden, G.S. Salvesen, Intrinsic cleavage of receptor-interacting protein kinase-1 by caspase-6, *Cell Death Differ.* 20 (1) (2013) 86–96.
- [105] A. Angel, R. Volkman, T.G. Royal, D. Offen, Caspase-6 knockout in the 5xFAD model of Alzheimer's disease reveals favorable Outcome on memory and Neurological hallmarks, *Int. J. Mol. Sci.* 21 (3) (2020).
- [106] R.A. Bennett, D.M. Wilson 3rd, D. Wong, B. Demple, Interaction of human apurinic endonuclease and DNA polymerase beta in the base excision repair pathway, *Proc Natl Acad Sci U S A* 94 (14) (1997) 7166–7169.
- [107] P. Sykora, M. Misiak, Y. Wang, S. Ghosh, G.S. Leandro, D. Liu, J. Tian, B.A. Baptiste, W.N. Cong, B.M. Brennerman, et al., DNA polymerase beta deficiency leads to neurodegeneration and exacerbates Alzheimer disease phenotypes, *Nucleic Acids Res.* 43 (2) (2015) 943–959.
- [108] M.A. Lovell, W.R. Markesbery, Oxidative DNA damage in mild cognitive impairment and late-stage Alzheimer's disease, *Nucleic Acids Res.* 35 (22) (2007) 7497–7504.
- [109] S. Merlo, L. Basile, M.L. Giuffrida, M.A. Sortino, S. Guccione, A. Copani, Identification of 5-Methoxyflavone as a novel DNA polymerase-beta inhibitor and neuroprotective agent against beta-amyloid toxicity, *J Nat Prod* 78 (11) (2015) 2704–2711.
- [110] L. Meng, M. He, M. Xiong, X. Zhang, S. Nie, J. Xiong, D. Hu, Z. Zhang, L. Mao, Z. Zhang, 2',3'-Dideoxycytidine, a DNA polymerase-beta inhibitor, Reverses memory deficits in a mouse model of Alzheimer's disease, *J Alzheimers Dis* 67 (2) (2019) 515–525.
- [111] A. Copani, J.J. Hoozemans, F. Caraci, M. Calafiore, E.S. Van Haastert, R. Veerhuis, A.J. Rozemuller, E. Aronica, M.A. Sortino, F. Nicoletti, DNA polymerase-beta is expressed early in neurons of Alzheimer's disease brain and is loaded into DNA replication forks in neurons challenged with beta-amyloid, *J. Neurosci.* 26 (43) (2006) 10949–10957.
- [112] F. Caraci, A. Fidilio, R. Santangelo, G. Caruso, M.L. Giuffrida, M.F. Tomasello, F. Nicoletti, A. Copani, Molecular connections between DNA replication and cell death in beta-amyloid-Treated neurons, *Curr. Neuropharmacol.* 21 (9) (2023) 2006–2018.
- [113] Y. Xiang, M.F. Goodman, W.A. Beard, S.H. Wilson, A. Warshel, Exploring the role of large conformational changes in the fidelity of DNA polymerase beta, *Proteins* 70 (1) (2008) 231–247.
- [114] J.L. Yang, W.Y. Chen, Y.P. Chen, C.Y. Kuo, S.D. Chen, Activation of GLP-1 receptor enhances neuronal base excision repair via PI3K-AKT-induced expression of apurinic/Pyrimidinic endonuclease 1, *Theranostics* 6 (12) (2016) 2015–2027.
- [115] J. Zhou, J. Ahn, S.H. Wilson, C. Prives, A role for p53 in base excision repair, *EMBO J.* 20 (4) (2001) 914–923.
- [116] D. Rea, V. Fulop, Structure-function properties of prolyl oligopeptidase family enzymes, *Cell Biochem. Biophys.* 44 (3) (2006) 349–365.
- [117] P.T. Mannisto, J.A. Garcia-Horsman, Mechanism of action of prolyl oligopeptidase (PREP) in Degenerative brain diseases: has peptidase activity only a modulatory role on the interactions of PREP with proteins? *Front. Aging Neurosci.* 9 (2017) 27.
- [118] X.Y. Chen, Y.F. Du, L. Chen, Neuropeptides exert neuroprotective effects in Alzheimer's disease, *Front. Mol. Neurosci.* 11 (2018) 493.
- [119] M.J. Hannula, T.T. Myohanen, J. Tenorio-Laranga, P.T. Mannisto, J.A. Garcia-Horsman, Prolyl oligopeptidase colocalizes with alpha-synuclein, beta-amyloid, tau protein and astroglia in the post-mortem brain samples with Parkinson's and Alzheimer's diseases, *Neuroscience* 242 (2013) 140–150.
- [120] R. Svarcbahs, U. Julku, T. Kilpelainen, M. Kyyro, M. Jantti, T.T. Myohanen, New tricks of prolyl oligopeptidase inhibitors - a common drug therapy for several neurodegenerative diseases, *Biochem. Pharmacol.* 161 (2019) 113–120.
- [121] V. Fulop, Z. Bocskei, L. Polgar, Prolyl oligopeptidase: an unusual beta-propeller domain regulates proteolysis, *Cell* 94 (2) (1998) 161–170.